Somite division and new boundary formation by mechanical strain

Nelemans, B.K.A.; Schmitz, M.; Tahir, H.; Merks, R.M.H.; Smit, T.H.

iScience

CellPress
OPEN ACCESS

Article

Somite Division and New Boundary Formation by Mechanical Strain

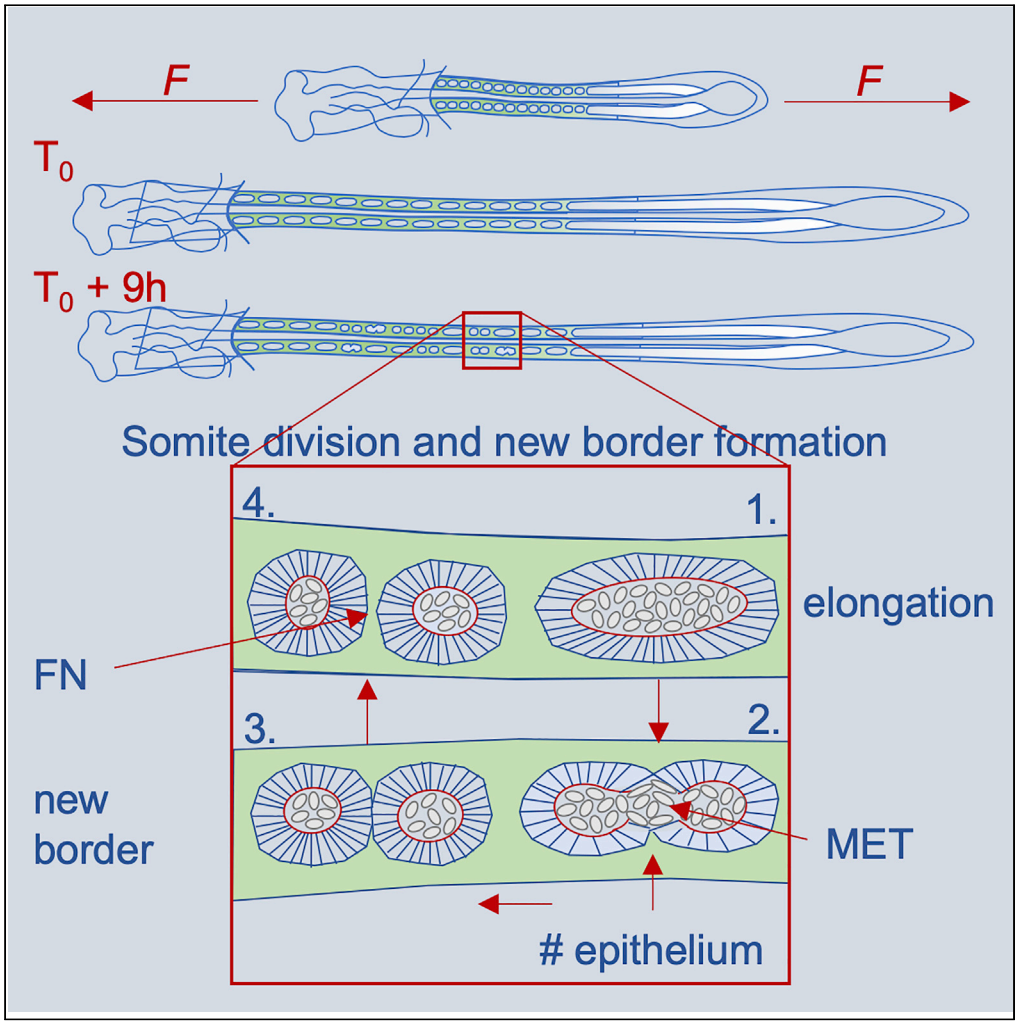

Ben K.A. Nelemans, Manuel Schmitz, Hannan Tahir, Roeland M.H. Merks, Theodoor H. Smit

th.smit@amsterdamumc.nl

HIGHLIGHTS

Live chick embryos develop normally under substantial axial strain (>50%)

Mature somites divide into daughter somites, and fibronectin is deposited in between

Mesenchymal cells from the somitocoel transition into epithelial border cells

Mechanical strain can induce border formation and thus affect morphogenesis

Nelemans et al., iScience *23*, 100976
April 24, 2020
https://doi.org/10.1016/j.isci.2020.100976

iScience

CellPress
OPEN ACCESS

Article

Somite Division and New Boundary Formation by Mechanical Strain

Ben K.A. Nelemans,[1,6,9] Manuel Schmitz,[1,7,8] Hannan Tahir,[1,2,8] Roeland M.H. Merks,[2,3,5] and Theodoor H. Smit[1,4,10,*]

SUMMARY

Somitogenesis, the primary segmentation of the vertebrate embryo, is associated with oscillating genes that interact with a wave of cell differentiation. The necessity of cell-matrix adherence and embryonic tension, however, suggests that mechanical cues are also involved. To explicitly investigate this, we applied surplus axial strain to live chick embryos. Despite substantial deformations, the embryos developed normally and somite formation rate was unaffected. Surprisingly, however, we observed slow cellular reorganizations of the most elongated somites into two or more well-shaped daughter somites. In what appeared to be a regular process of boundary formation, somites divided and fibronectin was deposited in between. Cell counts and morphology indicated that cells from the somitocoel underwent mesenchymal-epithelial transition; this was supported by a Cellular Potts model of somite division. Thus, although somitogenesis appeared to be extremely robust, we observed new boundary formation in existing somites and conclude that mechanical strain can be morphologically instructive.

INTRODUCTION

During morphogenesis, cells and tissues are subject to mechanical forces. These are generated by the cells themselves through cell-cell adhesion and contraction (Heer and Martin, 2017) and by external cues like osmotic pressure, growth, and forces generated by other cells. As cells are mechanosensitive, mechanical stress feeds back on cell behavior and can thus be considered instructive, e.g., as an organizing factor (Kumar et al., 2017) or as an activator of signaling pathways (Hubaud et al., 2017). This suggests that, alongside diffusible morphogens (Wolpert, 1969), mechanical strain is a provider of positional information (Miller and Davidson, 2013; Turing, 1952).

Somitogenesis involves the periodic organization of mesenchymal cells from the presomitic mesoderm (PSM) into cohesive clusters with an epithelial boundary. These clusters—somites—underlie the segmentation of the vertebrate body as they develop further into vertebrae and ribs, form the myotomes (the anlagen of the axial muscles), and impose segmentation on the peripheral nervous system. Somite formation is associated with genetic oscillations, which appear to be intrinsic to the cells of the PSM (Hubaud et al., 2017; Lauschke et al., 2012); this is described in the clock-and-wavefront model where molecular oscillators originating at the caudal end of the PSM (the clock) interact with a traveling front of maturation (the wave) created by antagonistic signaling gradients (Hubaud and Pourquié, 2014). The physical separation of a somite from the PSM correlates with the periodic expression of ephrin receptor A4 (EphA4) that interacts with ephrinB2 to induce cellular repulsion and cleft formation (Watanabe et al., 2009). This new boundary is then stabilized by the epithelization of the boundary cells (Martins et al., 2009) and the assembly of a fibronectin matrix in between (Rifes and Thorsteinsdóttir, 2012). Somite formation requires the condensation of cells in the PSM (Duess et al., 2013), the intercellular epithelial connection by N-cadherins (Horikawa et al., 1999), and cellular adhesion to the fibronectin surrounding the PSM (Georges-Labouesse et al., 1996; Martins et al., 2009). Somitogenesis is further facilitated by a tension on the embryo (Stern and Bellairs, 1984), which is naturally provided by the blastoderm that expands along the vitelline membrane (New, 1959). These studies indicate that not only molecular signaling, but also mechanical cues are involved in somite formation.

Considering then a possible role for mechanics in somitogenesis, we hypothesized that external mechanical strain might affect segmental patterning in the vertebrate embryo. Stern and Bellairs had inhibited the natural strain of live chick embryos by attaching them to a substrate; they observed a substantial widening

[1]Department of Orthopaedic Surgery, Amsterdam University Medical Centres, Amsterdam Movement Sciences, Meibergdreef 9, 1105AZ Amsterdam, the Netherlands

[2]Centrum Wiskunde & Informatica, Science Park 123, 1098 XG Amsterdam, the Netherlands

[3]Mathematical Institute Leiden, Leiden University, Niels Bohrweg 1, 2333 CA Leiden, the Netherlands

[4]Department of Medical Biology, Amsterdam University Medical Centres, Meibergdreef 9, 1105AZ Amsterdam, the Netherlands

[5]Present address: Mathematical Institute and Institute of Biology Leiden, Leiden University, Niels Bohrweg 1, 2333 CA Leiden, The Netherlands

[6]Present address: Developmental Biology, Department of Biology, Faculty of Science Utrecht University, Leuvenlaan 4, 3584 CE Utrecht, the Netherlands

[7]Present address: Fraunhofer-Institut für Werkstoffmechanik, Wöhlerstraße 11, 79108 Freiburg im Breisgau, Germany

[8]Present address: Department of Epidemiology, University Medical Centre Utrecht, Heidelberglaan 100, 3584 CX Utrecht, the Netherlands

[9]These authors contributed equally

[10]Lead Contact

*Correspondence: th.smit@amsterdamumc.nl

https://doi.org/10.1016/j.isci.2020.100976

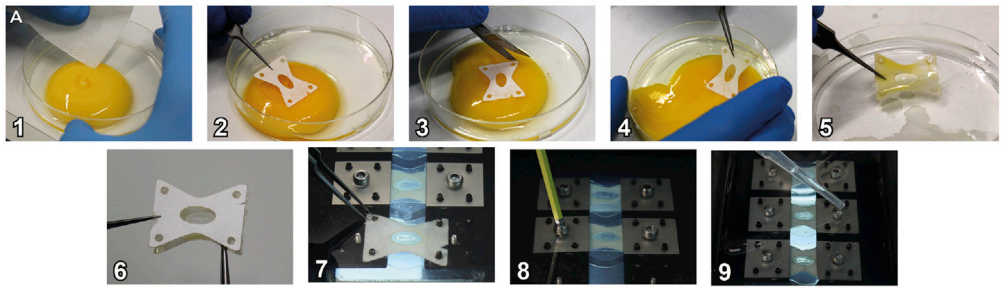

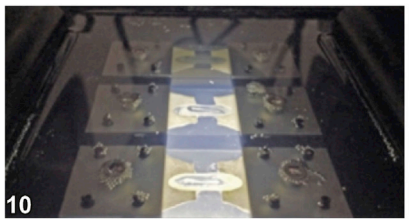

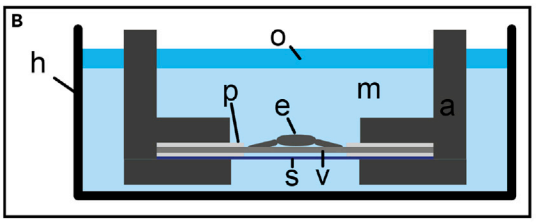

a metal arm
e embryo
f frame
h heated beaker
l lateral screws
m medium
o minderal oil
p filter paper
s silicone sheet
v vitelline membrane
w washer

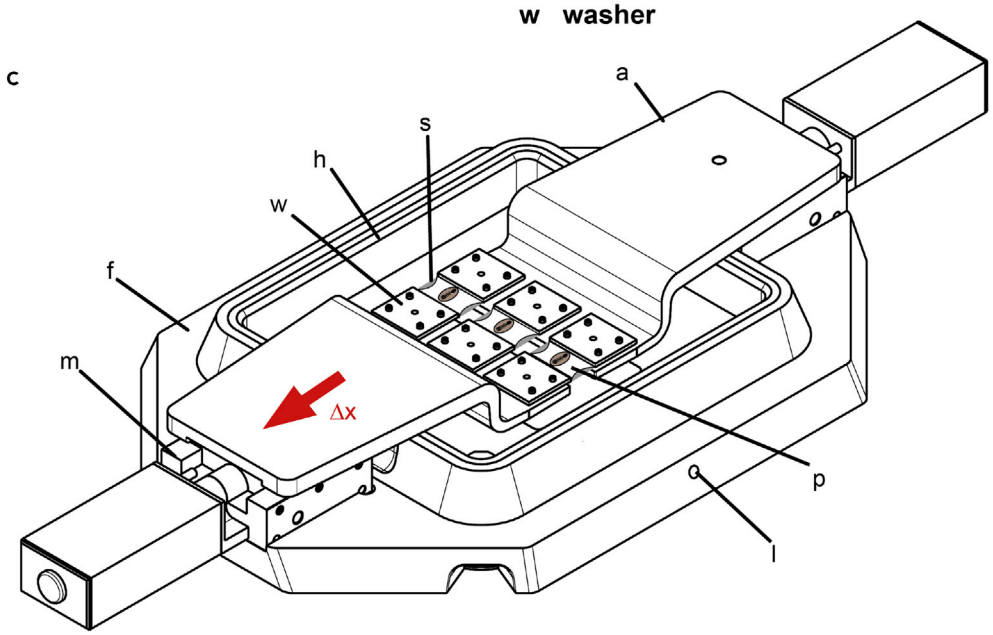

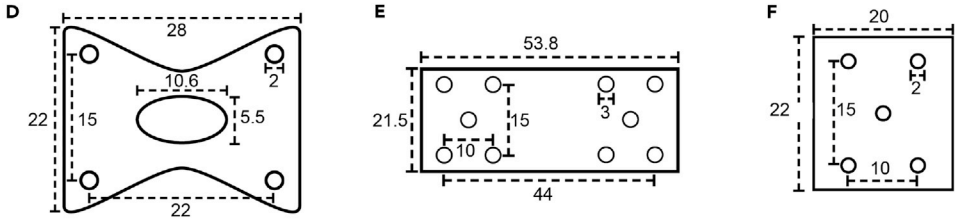

Figure 1. Chick Embryo Stretching *Ex Ovo*, Experimental Setup

(A) Procedure of chick embryo explantation (Schmitz et al., 2016). (1) An egg is cracked into Petri dish and thick albumen removed from top of the yolk. (2) A filter paper carrier is placed on top of the yolk, surrounding the blastoderm and a substantial area of the vitelline membrane. (3) The filter paper carrier is cut loose from the surrounding vitelline membrane and (4) removed from top of the yolk. (5) Remaining yolk is carefully washed away in a saline bath. (6) The embryo is sandwiched with a second filter paper carrier. (7) The filter paper sandwich is submerged into the medium and hooked into the pins of the motorized arms. A thin sheet of PDMS below the embryo and vitelline membrane protects the embryo from convection of the medium. (8) Washer plates clamp the filter paper sandwich to the metal arms and are carefully pressed down by nuts. (9) Filter paper sandwiches are cut perpendicularly at mid-level of the embryo for later stretching of embryos and the medium is covered with a layer of light mineral oil to prevent evaporation. (10) Three embryo sandwiches are pulled simultaneously under microscopic imaging to create time-lapses.

(B) Schematic cross-sectional view of the chick embryo (E) mounted along with the vitelline membrane (v) in a filter paper sandwich (p). The entire sandwich is supported by a flexible sheet of PDMS (s) and attached to the metal arms (A). The embryo is submerged in medium (m) in a heated beaker (H). A layer of mineral oil (o) prevents the medium from evaporating.

(C) Schematic view of the embryo stretcher. The frame carries the motorized stages and keeps the temperature-controlled medium container in position. The whole setup is placed on a motorized x-y-stage, embryos are imaged from above and illuminated from below through the glass bottom of the medium container.

(D) Filter paper carrier dimensions (in mm).

(E) Dimensions of stencil for PDMS sheets (in mm).

(F) Dimensions of metal washers used to clamp the filter paper (in mm).

of somites and eventually a secondary, lateral division (Stern and Bellairs, 1984). We applied a surplus longitudinal strain to the embryo, well beyond the natural tension of the blastoderm. We expected that such tension would induce a change in somite number or formation rate, but somitogenesis was essentially unaffected. Instead, and much to our surprise, the most elongated somites underwent slow subdivisions in what appeared to be a regular process of boundary formation, giving rise to what we designate as daughter somites. Here we report on these somite divisions and present a Cellular Potts model (CPM), which indicates that somite subdivisions may involve a mesenchymal to epithelial transition.

RESULTS

Embryo Stretching Protocol

Stage HH8-9 chick embryos were cultured *ex ovo* in modified submerged filter paper sandwiches (Figure 1) (Schmitz et al., 2016). They were stretched along their body axis in the filter paper sandwiches at a continuous rate of 8 μm/min, resulting in an elongation of the embryo of about 4 μm/min. After 16 h of elongation, we observed the division of somites for the first time. However, in this stretching protocol many of the embryo cultures were torn by the excessive tension, which impeded repeatability. To optimize the stretching protocol, we strained the embryos in two sessions of 51–55 min at 1.2 μm/s, separated by a resting period of 2 h, during which the samples could relax and repair (Figure S1). This protocol resulted in a sample elongation of 7.6 mm, equaling the 16 h of continuous stretching at 8 μm/min. The embryos themselves experienced strains of 23 ± 3% (average ±SD; n = 57) during the first pull and 19 ± 3% during the second pull, on top of the natural growth of the embryo and viscous relaxation (Figure S1). The total elongation of the embryos was around 70%–80% for the experimental group and 25%–30% for the controls (Figure S1). The variations in strain are due to variability in original embryo length and biological variation in stiffness of both embryo and the supporting membrane.

Somitogenesis Is Normal, but Somites Divide

After the second pull (t_0), we monitored the strained embryos for another 12 h. Time-lapse microscopic imaging revealed that somites budded off from the PSM with the same period in stretched samples (80 ± 6 min/somite) as in controls (79 ± 8 min/somite), but as expected the stretched somites were more elongated (Figure 2; Videos S1 and S2). Strikingly, however, the most deformed somites then divided into what we call "daughter somites" (Figure 2). During this process, the deformed mother somites invaginated along the medio-lateral plane (Figures 2E and 2F). This occurred simultaneously to or after their separation from the PSM and took more than 5 h (about four somite periods) from the first appearance of an invagination to complete boundary formation between the daughter somites.

Somite division in stretched embryos appeared unilaterally or bilaterally and often resulted in daughter somites of different sizes (Figures S2 and S3). Daughter somites consisting of only a few epithelial cells were also observed (Figure 3E).

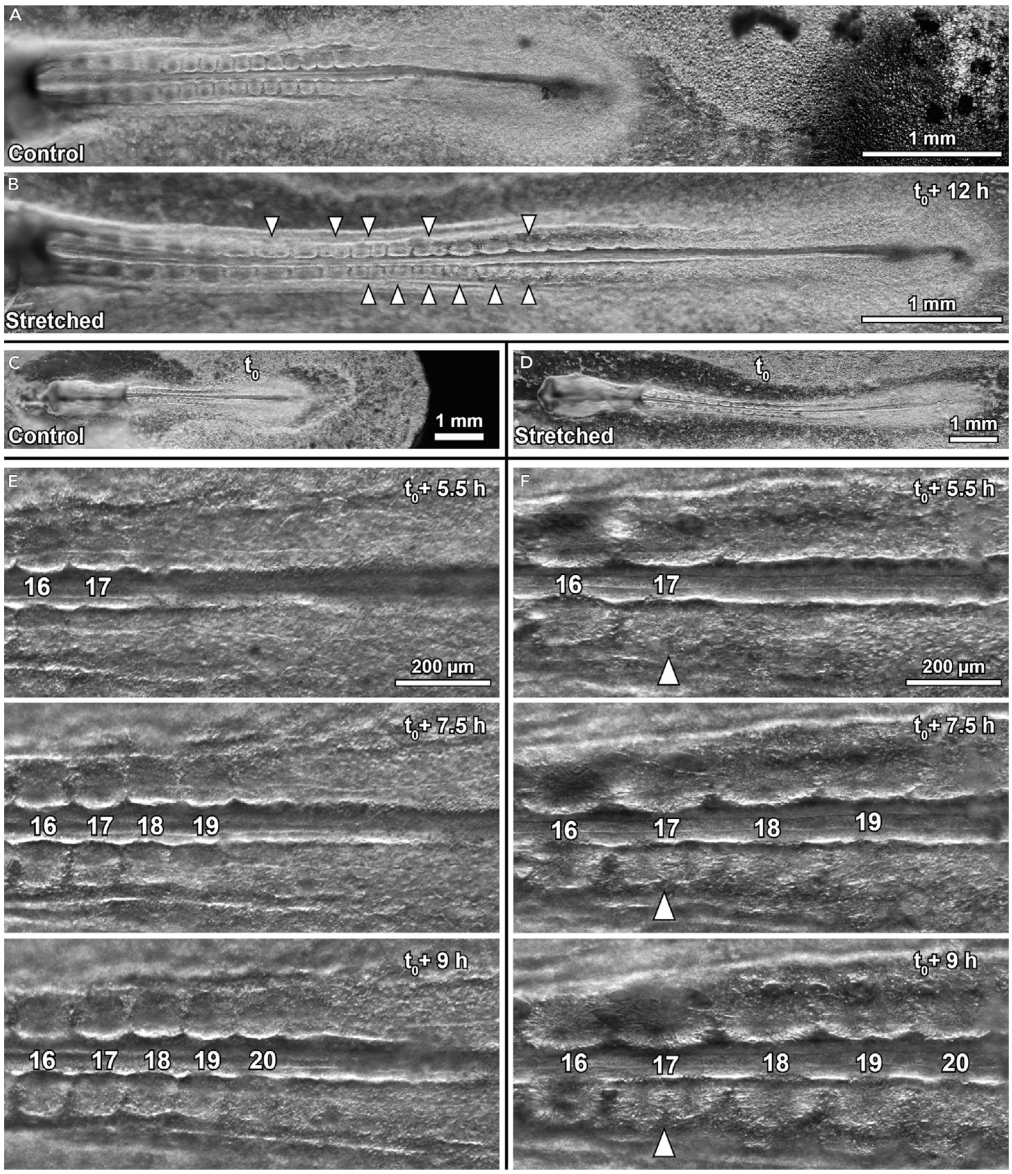

Figure 2. Daughter somite Formation in Stretched Chicken Embryos

Dark-field microscopy images of age-matched control (A) and stretched embryo (B). Anterior is to the left in all images, white arrowheads indicate daughter somite formation; t_0 marks the end of the stretching protocol (Figure S1), ventral view. Difference in axial length becomes obvious between control embryo (C) and stretched embryo (D) (at t_0 both embryos are at the 13-somite stage). Selected time-lapse frames of the segmenting PSM in control (E) and stretched embryo (F). The numbers in (E) and (F) indicate the total number of somites in the embryo, not the identity of the specific somites.

Daughter Somites Form New Epithelial Boundaries

We fixed and immunohistochemically stained the stretched embryos (Figures 3 and 4). Under wide-field microscopy, daughter somites appeared as stable, clearly separated cellular spheres enclosed by a fibrous extracellular matrix (ECM) staining positive for fibronectin (Figure 3, 4A, and 4B). Somites in control embryos were round (Figures 3A–3D), whereas those in stretched embryos were strongly deformed to an elliptical shape, with the epithelial cells organized radially around a somitocoel of mesenchymal cells (Figures 3E–3H). We identified potential transitional stages of daughter somite formation (Figures 4C–4G). The apical actin cortices of these somites showed discontinuities along their mediolateral planes, indicating openings of the epithelial sheet under mechanical strain (Figure S4). At these locations, mesenchymal cells from the somitocoel may integrate into the existing epithelium.

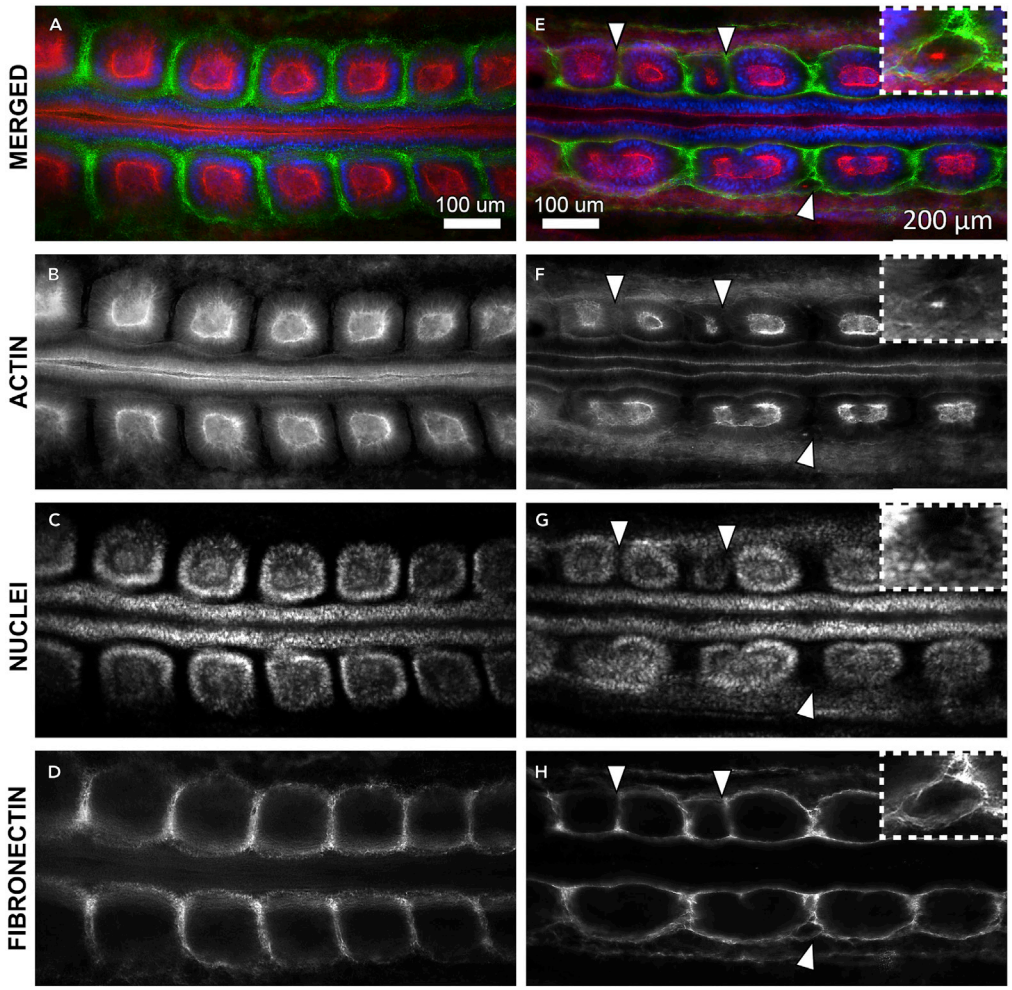

Figure 3. Fibronectin Distribution Around Daughter Somites

Widefield fluorescent micrographs of control embryo (A–D) and stretched embryo (E–H) stained for actin (red), DNA in cell nuclei (blue), and extracellular matrix component fibronectin (green). Ventral view, anterior is to the left. Daughter somites are surrounded and separated from each other by a newly formed fibronectin matrix (white arrowheads in [E] and [H]) and can be extremely small (inset [E]–[H]) and lacking a mesenchymal core. Photo credit: Ben Nelemans, Amsterdam University Medical Centres.

Mechanical Strain Appears to Activate EphA4, but Not Uncx4.1 or cMeso1

To determine whether mechanical strain re-activated genes related to somitic boundary formation, we stained for *EphA4* mRNA expression (Figures 4H and 4I). EphA4 is reported to induce somite detachment through the repulsion of ephrinb2 (Watanabe et al., 2009). *EphA4* was consistently expressed ectopically at the apical side of the epithelium of the stretched somites (Figure 4I), albeit at a much lower level than at somite 0 in both stretched and control somites (Figures 4H and 4I). There was no *EphA4* expression in the somites of the unstrained controls older than somite I (Figure 4H). Stretching did not affect the expression of *cMeso1* (Figures 4J and 4K), the key initiator of somite rostro-caudal polarity in chicken (Morimoto et al., 2007), or the expression of the caudal somite marker *Uncx4.1* (Schrägle et al., 2004) (Figures 4L and 4M); this indicates that the clock-and-wavefront mechanism is operating normally in stretched embryos.

Cellular Potts Model of Somite Division

In order to obtain a better understanding of the cellular reorganization during somite division, we developed a cell-based, two-dimensional CPM, implemented in the open-source package CompuCell3D (Glazier and Graner, 1993). The default hypothesis for the splitting of rod-shaped clusters of cohesive cells into a series of spherical aggregates is a mechanism known as the Plateau-Rayleigh instability (Hutson et al., 2008). This mechanism is

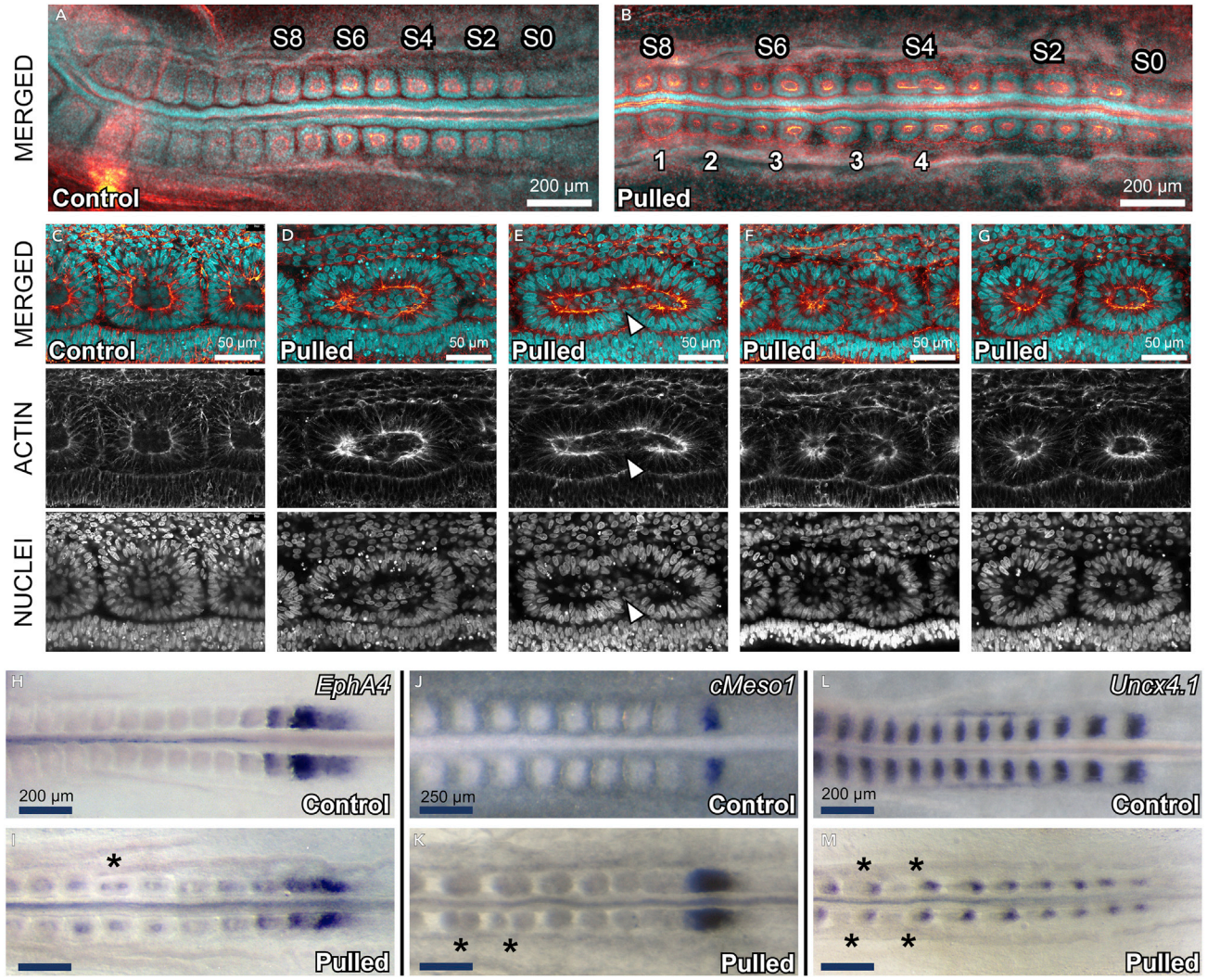

Figure 4. Immunohistochemistry and *In Situ* Hybridizations of the Embryos

(A and B) Control (A) and stretched embryo (B), anterior is left, somite numbers are indicated (Christ and Ordahl, 1995). Scale bars, 200 μm. (B) Daughter somites can form unilaterally (1), equally (4), or unequally sized (3) and subdivide further (2).

(C–G) Confocal cross sections of selected somites of the same control (C) and stretched embryo (D–G). Anterior is left and medial below. Panels are arranged in potential order to illustrate the transition from a mechanically deformed somite (D) to two daughter somites (G). Cells from the somitocoel seem to be incorporated into the epithelium at the site where the epithelium is ruptured (arrowhead in [E]).

(H–M) *In situ* hybridizations for *EphA4*, *cMeso1*, and *Uncx4.1* show that *EphA4* expression is maintained or induced around the somitocoels (I), whereas no new rostro-caudal polarity is induced in the daughter somites (indicated by *).

only possible in three dimensions, because in two dimensions there is no ring tension. Using viscous liquid models of tissue mechanics, Grima and Schnell argued that for typical values of the tissue surface tension and bulk viscosity of embryonic tissues, such surface-tension-driven mechanisms are likely not fast and strong enough to be the main driving forces of somite formation Grima and Schnell, 2007. Therefore, we turned to a more complex model, which we simulated in 2D for computational efficiency.

We initialized our simulations with a somite consisting of a core of non-polarized mesenchymal cells surrounded by a layer of polarized, epithelial cells (Dias et al., 2014), embedded in an elastic extracellular matrix (ECM; Figure 5A). We mimicked stretching by applying axial tension to the ECM (Video S3). Epithelial cells are mutually coupled by tight junctions, linked intracellularly to the cytoskeleton (Figure S5) (Kim et al., 2017). Elastic springs coupled the apical sides of the simulated epithelial cells to one another, whereas a set of intracellular springs represented the cytoskeleton (Figure S5) (Dias et al., 2014).

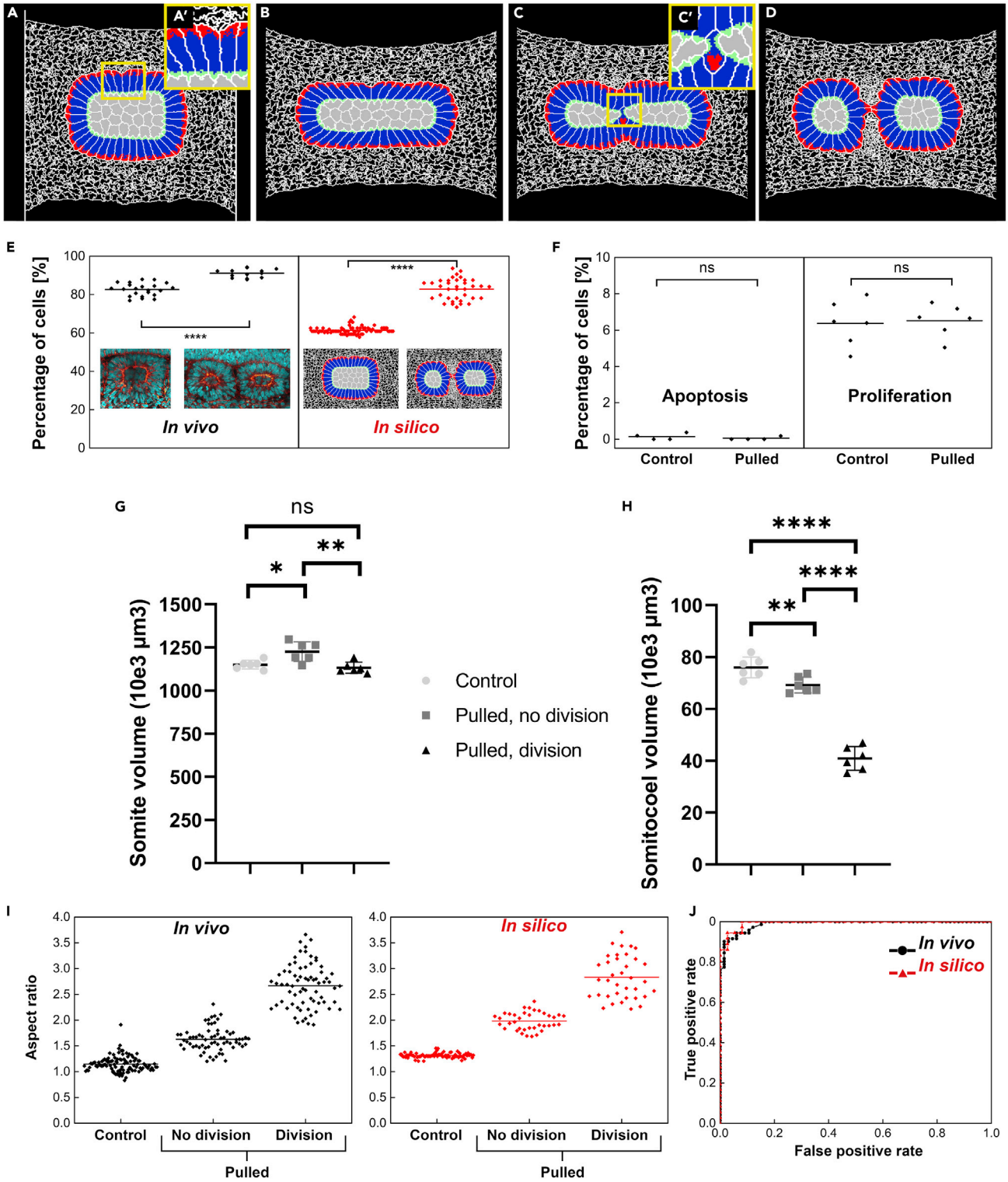

Figure 5. Cellular Potts Model of Somite Remodeling Compared with *In Vivo*

(A–D) Daughter somite formation *in silico*, induced by stretching. Mesenchymal cells (gray) and extracellular matrix (white mesh), (A′) epithelial cells consisting of apical (green), lateral (blue) and basal (red) domains. (C′) Somitocoel cells undergoing MET.

(E) There is a significant increase of epithelial cell fraction *in vivo* ($p < 0.0001$) and *in silico* ($p < 0.0001$).

Figure 5. *Continued*

(F) Apoptotic and proliferation rates in somitic mesoderm of control and stretched embryos; differences are non-significant (Mann-Whitney test, apoptosis $p = 0.43$, proliferation $p = 0.79$).

(G) Volumes of control (unstrained), strained, and daughter somites S5 and S6. Volumes of divided somites are summed from two daughter somites and show no significant volume difference to control somites. There is a temporary increase in volume, when somites are pulled, but have not yet divided. ns, not significant; *: $p<0.05$; **: $p<0.01$

(H) Somitocoel volumes in the same somites, showing a strong decrease of mesenchymal volume after somite splitting ($p < 0.0001$), thereby confirming mesenchymal-epithelial transition. **: $p<0.01$; ***: $p<0.001$; ****: $p<0.0001$.

(I) Somite aspect ratios for controls and non-divided and divided somites *in vivo* and *in silico*.

(J) ROC curves for daughter somite formation *in vivo* and *in silico*, in dependence of aspect ratio of deformed somites. AUC is 0.989 (*in vivo*, 95% confidence interval [CI]: 0.953–0.999) and 0.993 (*in silico*, 95% CI: 0.938–1.000). Dots in Figures 5E–5I are individual data points, the lines indicating their mean values. Figures 5G and 5H also include the Standard Error of the Mean (SEM).

MET May Occur through Lateral Induction of Broken Epithelium

First, we tested if stretching and reorganization of the mesenchymal and epithelial cells sufficed for somite division. However, none of the strains tested induced somite division (Figure S6, top row). Considering then that two daughter somites need more epithelial cells than one mother somite, we assumed that the mesenchymal cells from the somitocoel could transition into the epithelium, thus mimicking a mesenchymal-epithelial transition (MET). We tested two rules for inducing MET in the deformed somite. In the first scenario, a mesenchymal cell underwent MET after full migration into the epithelial layer and contact with the surrounding ECM for 600 time steps (counted in Monte Carlo Steps [MCS], see Methods), corresponding to approximately 4 min (see Table S1). We did not observe somite division for different levels of deformation, possibly because there was insufficient contact between mesenchymal somitocoel cells and the surrounding ECM (Figure S6, middle row). In the second scenario, mesenchymal cells underwent MET after extended (600 MCS or 4 min) contact with the basal or lateral membrane of the epithelial cells. Upon stretching, the connections between the epithelial cells snapped and the mesenchymal cells from the core became exposed to their lateral or basal membranes. This induced MET and the cells were integrated into the epithelial layer (Figure S6, lower row; Video S3). We also observed that a decreased cohesion between the lateral domains of epithelial cells resulted in subdivisions into small cell clusters of epithelioid morphology (Figure S7), similar to the subsomites observed in *N-Cadherin/cad11* double-homozygous mouse mutants (Horikawa et al., 1999).

Ratio of Mesenchymal/Epithelial Cells Decreased

Integration of the mesenchymal cells into the epithelial layer inherently increases the somite's surface-volume ratio. Also *in vivo* the epithelial cell fraction was significantly higher in daughter somites than in controls and matched the *in silico* prediction (Figure 5E). Importantly, the stretching *in vivo* caused no significant changes in apoptosis ($p = 0.4286$) or proliferation rates ($p = 0.7879$) (Figure 5F). We also compared the volumes of somites and somitocoels between control, stretched, and divided somites V and VI (Figures 5G and 5H). These quantifications show that stretched somites increase in volume before division. After division, however, the total volume of the daughter somites does not significantly differ from control somites, suggesting again that the same number of cells are kept during the cellular rearrangement and that the cell ratio is not related to any volumetric effect (Figure 5G). Finally, divided somitocoels show a ~50% smaller volume compared with control or stretched somites (Figure 5H). Altogether, the data suggest that MET is the most likely explanation for the observed increase in epithelial cell fraction.

Mechanical Deformation beyond Threshold Induces Somite Division

To determine the relationship between mechanical deformation of somites and the probability of somite division, we compared the aspect ratios of stretched dividing somites (prior to division) and stretched non-dividing somites with those of control somites (Figure 5I). These measurements show that somite division only occurs beyond an aspect ratio threshold of approximately 2.0 *in vivo* or 2.5 *in silico*. The corresponding receiver operating characteristics (ROC) curves (Hanley and McNeil, 1982) show that somite aspect ratio is indeed an excellent predictor of somite division, both *in vivo* and *in silico* (Figure 5J).

DISCUSSION

Vertebrates are characterized by their segmented body plan, first visible in the somites that form along the embryonic body axis. The numbers of somites and vertebrae are remarkably constant within species, although genetic mutations can slightly alter somite number and formation period (Schröter and Oates,

2010). Considering that morphogenesis is also a physical process, we hypothesized that mechanical strain might affect both the formation rate and the number of somites. In order to test this, we subjected chick embryos to a substantial mechanical strain, resulting in an elongation more than twice the natural lengthening of an embryo. Based on the stiffness (2.4 kPa) and size (84 by 200 μm) of the midline (notochord, neural tube, and somites) (Agero et al., 2010), a force of 8.4 μN is required to apply a strain of 23%. The stress applied on the midline after two pulls is about 1,200 Pa, well above the estimated yield stress in the anterior PSM (20–220 Pa) (Mongera et al., 2018) and apparently sufficient to break epithelial cell-cell adhesions.

Although the global forces applied are clearly supra-physiological, the average somite formation period remained essentially the same at approximately 80 min/somite. This shows that the clock-and-wavefront mechanism is extremely robust and not disturbed even by excessive mechanical strain. Surprisingly, however, beyond a threshold of somite deformation there was a slow reorganization of somites into two or more well-shaped daughter somites. Each division took about 6 h, similar to the period from the determination front (somite -IV) to the formation of somite I (Maroto et al., 2012). This indicates that daughter-somite formation is an active process of boundary formation, rather than an acute mechanical disruption.

Somite division starts with snapping of the somite epithelium, and one may wonder whether the process that follows is damage repair or normal morphogenesis. This is difficult to determine, because healing of biological tissues generally involves many processes that also occur during development. Furthermore, it is conceivable and in fact suggested (Bard, 1988; Truskinovsky et al., 2014) that local strains in the mesoderm may be several times the global embryo deformation due to differential straining. Indeed, the overstretching of a somite appears to create a situation that results in a morphogenetic process of new border formation. In this context it is interesting to note that the surplus strain applied to the live embryos affects cohesive (epithelial) cells in the anterior mesoderm (i.e., the somites), rather than the loose, granular (mesenchymal) cells in the PSM. This is commensurate with observations that cohesive granular materials crack under stretching, whereas dry, non-cohesive granules do not (Alarcón et al., 2010). It may also explain why somitogenesis, which essentially occurs in the mesenchymal PSM, is robust under supra-physiological strain and indeed may be insensitive to it.

Our mathematical modeling and microscopic observations suggest that the daughter somites are essentially composed of cells from the mother somite. This is confirmed by the observation that proliferation and apoptosis did not change under mechanical stretching. It further implies that the larger number of epithelial cells required to meet the demand of more border cells is met by mesenchymal-epithelial transition (MET). Both *in vivo* and *in silico* we observed that mechanical strain ruptured the apical actin cortices. The mesenchymal cells from the somite core come into contact with the lateral sides of the epithelial cells and presumably undergo mesenchymal-epithelial transitions (MET) (Jackson et al., 2017) to be integrated into the somitic epithelium. The ability of mesenchymal cells to revert to an epithelial identity demonstrates cell plasticity as suggested earlier (Dongre and Weinberg, 2019; Yang and Weinberg, 2008); our observations of somite divisions shows that interconversion between epithelial and mesenchymal cell states may also occur under mechanical conditions.

In situ hybridization for the Mesp2 homolog, Meso1, indicates that the clock-and-wavefront mechanism is operating normally in stretched embryos, presumably because mechanical strain does not affect loose, granular tissues like the mesenchyme of the PSM (Alarcón et al., 2010). We further consistently observed light ectopic expression of *EphA4* without *cMeso1* expression in the strained somites, although *EphA4* is thought to be downstream of *cMeso1* (Watanabe et al., 2009). Thus, somite division occurs without Meso1 expression defining the somitic border, as normally occurs during somitogenesis. This would indicate that *EphA4* expression in stretched somites is either maintained or reinitiated and suggests an alternative mechanosensitive pathway leading to EphA4 upregulation, independent from, or redundant to, *cMeso1*. However, we are hesitant to draw such firm conclusions, because the level of *EphA4* expression is much lower than observed in somite 0 in both the experimental and the control somites.

In 1984, Stern and Bellairs cultured chick embryos on agar-glucose-saline-albumen substrates, which in several cases inhibited their elongation and resulted in a PSM wider than normal (Stern and Bellairs, 1984). This PSM segmented in a normal rostral-caudal sequence, but the laterally elongated somites then subdivided secondarily into daughter somites of about normal size, that is, perpendicular to the direction of the maturation gradients. This indicates that boundary formation is induced independent

from any clock-and-wavefront mechanism. It further appears that "wide" somites formed under compression are unstable, commensurate to the "long" somites produced under tension in the current study. We observed that the epithelial layer of the elongated somite ruptured and induced mesenchymal-epithelial transition of the somitocoel cells (Jackson et al., 2017). Whether the epithelial layer of the wide somites in Stern and Bellairs' study also ruptured under axial compression cannot be determined from the figures in the publication, but considering their strong lateral elongation with estimated aspect ratios well above 2.0, this is quite conceivable.

Daughter somite formation, both under tension and compression, suggest that boundary formation can take place outside the somite determination front (Hubaud and Pourquié, 2014), presumably in response to mechanical cues, and thus independently from the clock-and-wavefront mechanism. This was also the case with the extra-embryonic *de novo* formation of somites (Dias et al., 2014): like normal somites, these ectopic somites had epithelial layers surrounding mesenchymal cells and were embedded in a matrix of fibronectin, which is known to be an essential condition for somite formation (Rifes and Thorsteinsdóttir, 2012). Unlike the situation in the compressed or elongated embryos, however, there were no geometrical boundary conditions for the ectopic somites imposed by the surrounding structures, which allowed the reported unrestricted, grape-like somite formation in all directions. An alternative explanation for the somite division reported here and the ectopic somite formation reported by Dias et al. (2014) is offered by Horikawa and colleagues, who created N-Cadherin mutations in chick embryos and observed small, irregular somites, which they called *subsomites* (Horikawa et al., 1999). We used our CPM to investigate the role of cadherins *in silico* and found that reduced intercellular adhesion indeed results in small, irregular subsomites (Figure S7). In our experimental study, however, daughter somites were not created by reducing cellular adherence but by mechanical overstraining of the epithelial border of the somites; the feasibility of this mechanism was confirmed by the CPM (Figure 5). The mechanism of ectopic somite formation (Dias et al., 2014) is as yet less clear and in fact out of scope of the current study. Based on the current study we conclude that mechanical strain can induce border formation and thus control morphogenesis; this is an important concept to keep in mind when studying not only embryonic development, but also tissue homeostasis and disease.

Limitations of the Study

Our study involves some limitations, which may be addressed in future studies. First, the straining protocol of two supra-physiological pulls, separated by 2 h of relaxation, looks quite arbitrary. Although we feel that a minimum of axial stretching is required to deform the somites and induce division and MET, other stretching regimes may have worked as well or even better. Alternatively, one may think about other (more physiological) ways to enhance differential strain between the rupturing epithelium and the surrounding tissues, connected to each other by fibronectin, e.g., by enhancing epithelial contraction.

Although our observations on border formation are robust and consistent, the case for MET would have been stronger if MET could have been shown in single cells. One way of doing that would be monitoring single mesenchymal cells of the somitocoel throughout the process of somite division, e.g., through DiI labeling of mesenchymal cells prior to stretching (Kulesa and Fraser, 2002). Alternatively, immunohistochemistry of single somites could highlight specific markers of MET or the epithelium. In our experimental setup this was technically not feasible because of the large, and somewhat unpredictable, displacement of somites prior to and during the stretching protocol.

METHODS

All methods can be found in the accompanying Transparent Methods supplemental file.

DATA AND CODE AVAILABILITY

All data needed to evaluate the conclusions in the paper are present in the paper and/or the Transparent Methods. All data and the computational modeling code are available from authors upon request.

SUPPLEMENTAL INFORMATION

Supplemental Information can be found online at https://doi.org/10.1016/j.isci.2020.100976.

ACKNOWLEDGMENTS

We are grateful to Julio Belmonte for his advice on the simulations at the early stages of model development. Stuart A. Newman and Frietson Galis made helpful comments to earlier versions of the manuscript.

B.K.A.N., M.S., and H.T. were financed by ZonMW-VICI grant 918.11.635 granted to T.H.S. R.M.H.M. was financially supported by NWO/ALW-VIDI grant 864.10.009 and NWO/ENW-VICI grant 865.17.004 granted to R.M.H.M.

AUTHOR CONTRIBUTIONS

Conceptualization, T.H.S. and R.M.H.M.; Methodology, B.K.A.N., M.S., T.H.S.; Software, H.T. and R.M.H.M.; Investigation, B.K.A.N., M.S. and H.T.; Writing – Original Draft, B.K.A.N. and M.S.; Writing – Review & Editing, R.M.H.M. and T.H.S.; Funding Acquisition, T.H.S.; Resources, T.H.S. and R.M.H.M.; Supervision, T.H.S. and R.M.H.M.

DECLARATION OF INTERESTS

The authors declare no competing interests.

Received: October 31, 2019
Revised: January 30, 2020
Accepted: March 9, 2020
Published: April 24, 2020

REFERENCES

Agero, U., Glazier, J.A., and Hosek, M. (2010). Bulk elastic properties of chicken embryos during somitogenesis. Biomed. Eng. Online *9*, 19.

Alarcón, H., Ramos, O., Vanel, L., Vittoz, F., Melo, F., and Géminard, J.C. (2010). Softening induced instability of a stretched cohesive granular layer. Phys. Rev. Lett. *105*, 208001.

Bard, J.B.L. (1988). A traction-based mechanism for somitogenesis in the chick. Roux's Arch. Dev. Biol. *197*, 513–517.

Christ, B., and Ordahl, C.P. (1995). Early stages of chick somite development. Anat.Embryol. (Berl.) *191*, 381–396.

Dias, A.S., de Almeida, I., Belmonte, J.M., Glazier, J.A., and Stern, C.D. (2014). Somites without a clock. Science *343*, 791–795.

Dongre, A., and Weinberg, R.A. (2019). New insights into the mechanisms of epithelial–mesenchymal transition and implications for cancer. Nat. Rev. Mol. Cell Biol. *20*, 69–84.

Duess, J.W., Fujiwara, N., Corcionivoschi, N., Puri, P., and Thompson, J. (2013). ROCK inhibitor (Y-27632) disrupts somitogenesis in chick embryos. Pediatr. Surg. Int. *29*, 13–18.

Georges-Labouesse, E.N., George, E.L., Rayburn, H., and Hynes, R.O. (1996). Mesodermal development in mouse embryos mutant for fibronectin. Dev. Dyn. *207*, 145–156.

Glazier, J.A., and Graner, G. (1993). Simulation of the differential adhesion driven rearrangement of biological cells. Phys. Rev. E. Stat. Phys. Plasmas Fluids Relat. Interdiscip. Top. *47*, 2128–2154.

Grima, R., and Schnell, S. (2007). Can tissue surface tension drive somite formation? Dev.Biol. *307*, 248–257.

Hanley, A.J., and McNeil, J.B. (1982). The meaning and use of the area under a receiver operating characteristic (ROC) curve. Radiology *143*, 29–36.

Heer, N.C., and Martin, A.C. (2017). Tension, contraction and tissue morphogenesis. Development *144*, 4249–4260.

Horikawa, K., Radice, G., Takeichi, M., and Chisaka, O. (1999). Adhesive subdivisions intrinsic to the epithelial somites. Situ *215*, 182–189.

Hubaud, A., and Pourquié, O. (2014). Signalling dynamics in vertebrate segmentation. Nat. Rev. Mol. Cell Biol. *15*, 709–721.

Hubaud, A., Regev, I., Mahadevan, L., and Pourquié, O. (2017). Excitable dynamics and Yap-dependent mechanical cues drive the segmentation clock. Cell *171*, 668–682.e11.

Hutson, M., Brodland, G., Yang, J., and Viens, D. (2008). Cell sorting in three dimensions: topology, fluctuations, and fluidlike instabilities. Phys. Rev. Lett. *101*, 148105.

Jackson, T.R., Kim, H.Y., Balakrishnan, U.L., Stuckenholz, C., and Davidson, L.A. (2017). Spatiotemporally controlled mechanical cues drive progenitor mesenchymal-to-epithelial transition enabling proper heart formation and function. Curr. Biol. *27*, 1326–1335.

Kim, H.Y., Jackson, T.R., and Davidson, L.A. (2017). On the role of mechanics in driving mesenchymal-to-epithelial transitions. Semin. Cell Dev. Biol. *67*, 113–122.

Kulesa, P.M., and Fraser, S.E. (2002). Cell dynamics during somite boundary formation revealed by time-lapse analysis. Science *298*, 991–995.

Kumar, A., Placone, J.K., and Engler, A.J. (2017). Understanding the extracellular forces that determine cell fate and maintenance. Development *144*, 4261–4270.

Lauschke, V.M., Tsiairis, C.D., François, P., and Aulehla, A. (2012). Scaling of embryonic patterning based on phase-gradient encoding. Nature *493*, 101–105.

Maroto, M., Bone, R.A., and Dale, J.K. (2012). Somitogenesis. Development *139*, 2453–2456.

Martins, G.G., Rifes, P., Amândio, R., Rodrigues, G., Palmeirim, I., and Thorsteinsdóttir, S. (2009). Dynamic 3D cell rearrangements guided by a fibronectin matrix underlie somitogenesis. PLoS One *4*, e7429.

Miller, C.J., and Davidson, L. (2013). The interplay between cell signalling and mechanics in developmental processes. Nat. Rev. Genet. *14*, 733–744.

Mongera, A., Rowghanian, P., Gustafson, H.J., Shelton, E., Kealhofer, D.A., Carn, E.K., Serwane, F., Lucio, A.A., Giammona, J., and Campàs, O. (2018). A fluid-to-solid jamming transition underlies vertebrate body axis elongation. Nature *561*, 401–405.

Morimoto, M., Sasaki, N., Oginuma, M., Kiso, M., Igarashi, K., Aizaki, K., Kanno, J., and Saga, Y. (2007). The negative regulation of Mesp2 by mouse Ripply2 is required to establish the rostro-caudal patterning within a somite. Development *134*, 1561–1569.

New, D. (1959). The adhesive properties and expansion of the chick blastoderm. J. Embryol. Exp. Morphol. *7*, 146–164.

Rifes, P., and Thorsteinsdóttir, S. (2012). Extracellular matrix assembly and 3D

organization during paraxial mesoderm development in the chick embryo. Dev. Biol. *368*, 370–381.

Schmitz, M., Nelemans, B., and Smit, T.H. (2016). A submerged filter paper sandwich for long-term ex ovo time-lapse imaging of early chick embryos. J. Vis. Exp. 54636.

Schrägle, J., Huang, R., Christ, B., and Pröls, F. (2004). Control of the temporal and spatial Uncx4.1 expression in the paraxial mesoderm of avian embryos. Anat. Embryol. (Berl). *208*, 323–332.

Schröter, C., and Oates, A.C. (2010). Segment number and axial identity in a segmentation clock period mutant. Curr. Biol. *20*, 1254–1258.

Stern, C.D., and Bellairs, R. (1984). The roles of node regression and elongation of the area pellucida in the formation of somites in avian embryos. J. Embryol. Exp. Morphol. *81*, 75–92.

Truskinovsky, L., Vitale, G., and Smit, T.H. (2014). A mechanical perspective on vertebral segmentation. Int. J. Eng. Sci. *83*, 124–137.

Turing, A.M. (1952). The chemical basis of morphogenesis. Philos. Trans. R. Soc. Lond. Ser. B Biol. Sci. *237*, 37–72.

Watanabe, T., Sato, Y., Saito, D., Tadokoro, R., and Takahashi, Y. (2009). EphrinB2 coordinates the formation of a morphological boundary and cell epithelialization during somite segmentation. Proc. Natl. Acad. Sci. U S A *106*, 7467–7472.

Wolpert, L. (1969). Positional information and the spatial pattern of cellular differentiation. J. Theor. Biol. *25*, 1–47.

Yang, J., and Weinberg, R.A. (2008). Epithelial-mesenchymal transition: at the crossroads of development and tumor metastasis. Dev. Cell *14*, 818–829.

iScience, Volume *23*

Supplemental Information

Somite Division and New Boundary Formation by Mechanical Strain

Ben K.A. Nelemans, Manuel Schmitz, Hannan Tahir, Roeland M.H. Merks, and Theodoor H. Smit

Supplemental Information

Supplemental figures

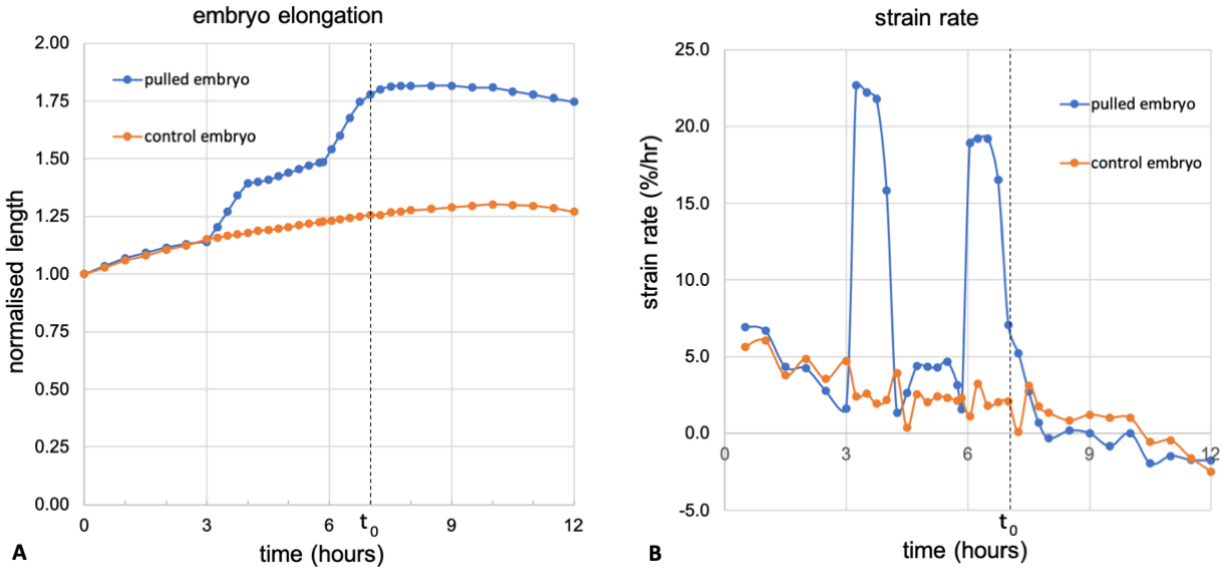

Fig S1: Natural and experimental elongation of chick embryos, related to figures 1 and 2, and Movies S1 and S2.
Left: embryo elongation normalized to the length at T=0. Right: strain rate (%/hr) for the same embryos. Orange: natural growth of the chick embryo is more than 25% after 9 hours. Elongation gradually slows down as embryo reaches the borders of the framed membrane (see also negative slope right). Blue: embryo pulled about 23% at T=3h, two hours rest, and again for 19% just before T=6h. The post-stretch period (t_0, see Fig.2) starts at T=7h. Total elongation including growth reaches 80% at T=8h. Note that the applied stretch does not affect the underlying elongation rate due to growth (negative slope similar to control embryo).

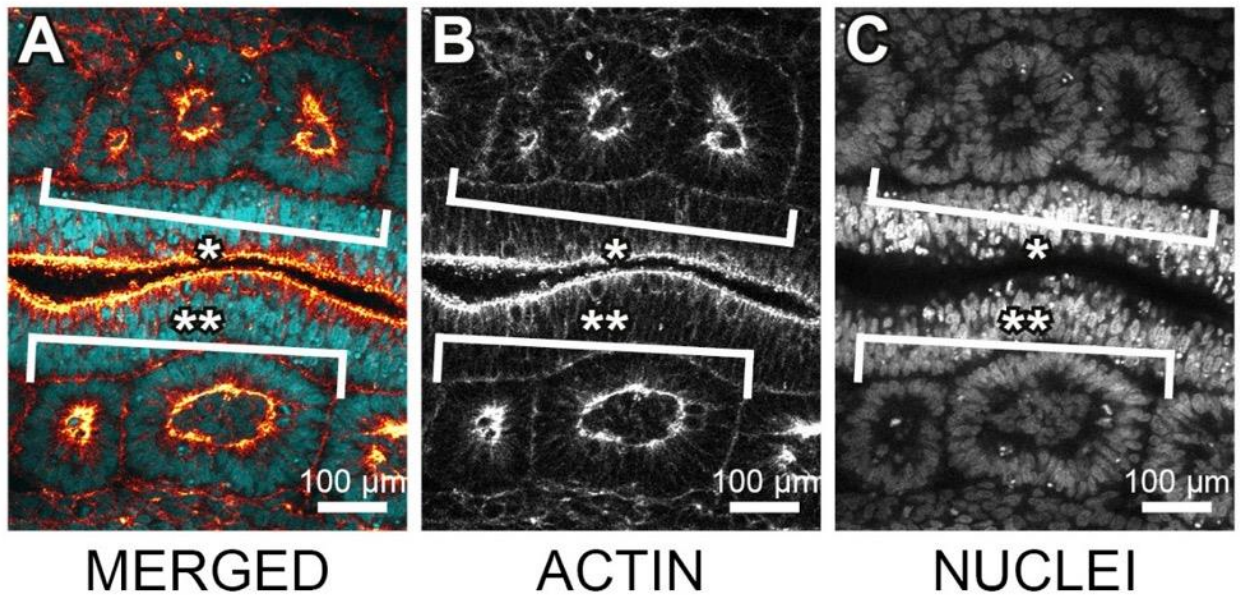

Fig S2: Versatile daughter somite morphologies, related to Figure 3. Confocal micrograph of daughter somites on both sides of the midline in stretched and fixated chick embryo stained for actin (red) and DNA in cell nuclei (blue). Anterior is to the left, ventral view. Daughter somites do not only result from splitting into anterior and posterior compartment of original somite, but can also reorganize into three daughter somites (*) or two unequally sized daughter somites (**).

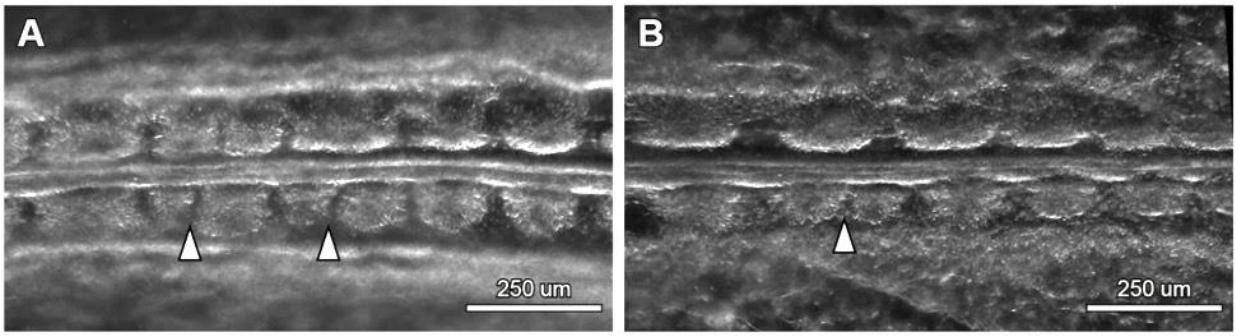

Fig S3: Unequally sized daughter somites, related to Figure 3. Anterior is to the left. White arrowheads indicate gaps between unequal daughter somite pairs.

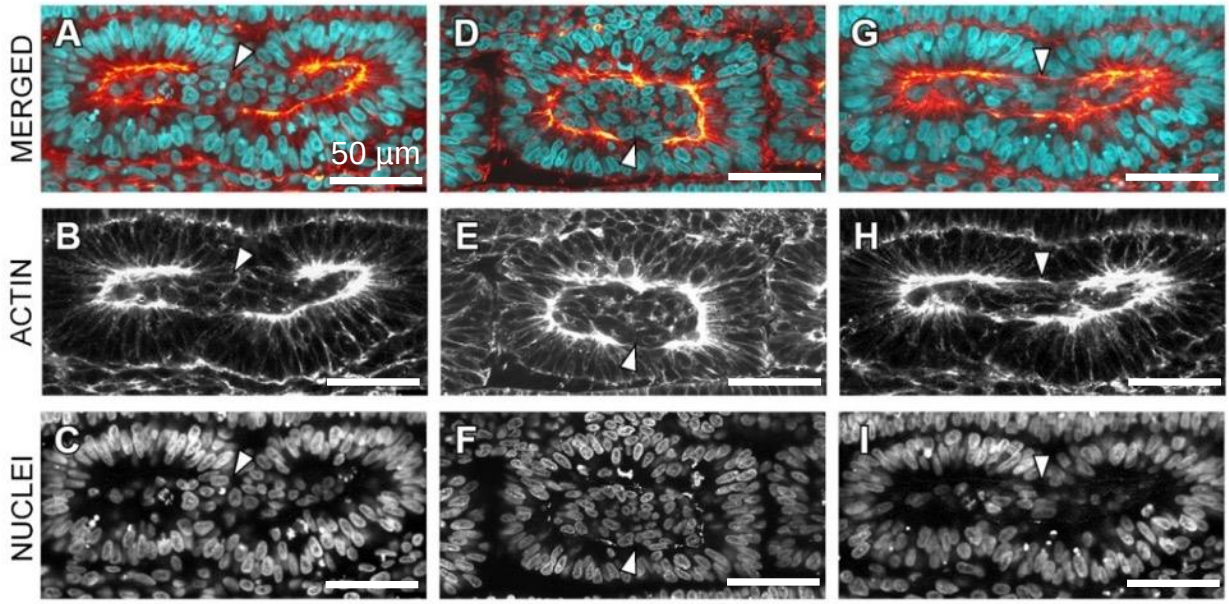

Fig S4: Fracture of epithelial sheet and potential MET of mesenchymal somitocoel cells, related to Figure 4. Confocal micrograph of somites, fixated during daughter somite formation in stretched chick embryos, stained for actin (orange) and DNA in cell nuclei (cyan). Anterior is to the left. White arrowheads indicate discontinuities in the apical actin ring of the somitic epithelium, suggesting a local opening of the epithelial sheet and potential interfaces for the recruitment of additional mesenchymal cells from the somitocoel for their incorporation into the existing epithelium.

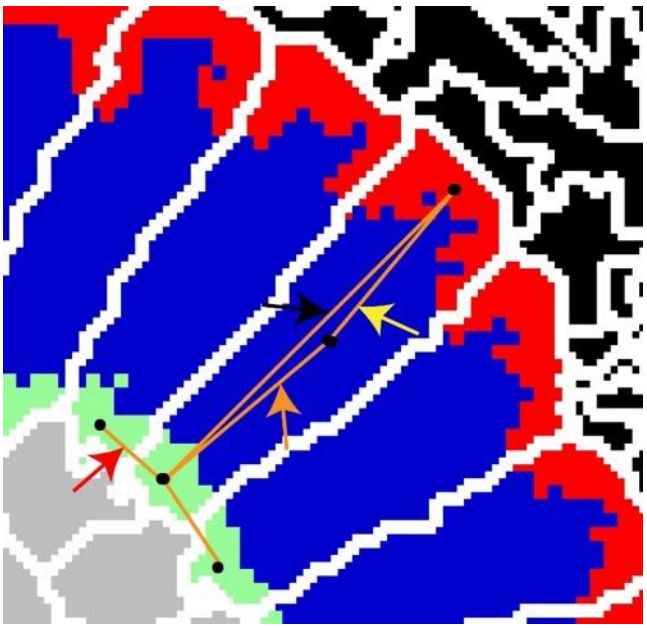

Fig S5: Snapshot of various cell types present in the simulations, related to Figure 5. Mesenchymal cells shown in grey. Epithelial cells consist of three domains: Apical (green), lateral (blue) and basal (red) domain. Centre of masses (black dots) of epithelial cell domains are connected internally to each other using elastic springs. The springs between apical and lateral domain (orange arrow), lateral and basal domain (yellow arrow) and apical and basal domain (black arrow) are indicated. Each epithelial cell has the same spring configuration helping epithelial cells to elongate after polarization. Apical domains of neighbouring are also connected via springs (red arrow) to trigger the formation of single layer of epithelial cells. Black cells in the upper right-hand corner represent ECM.

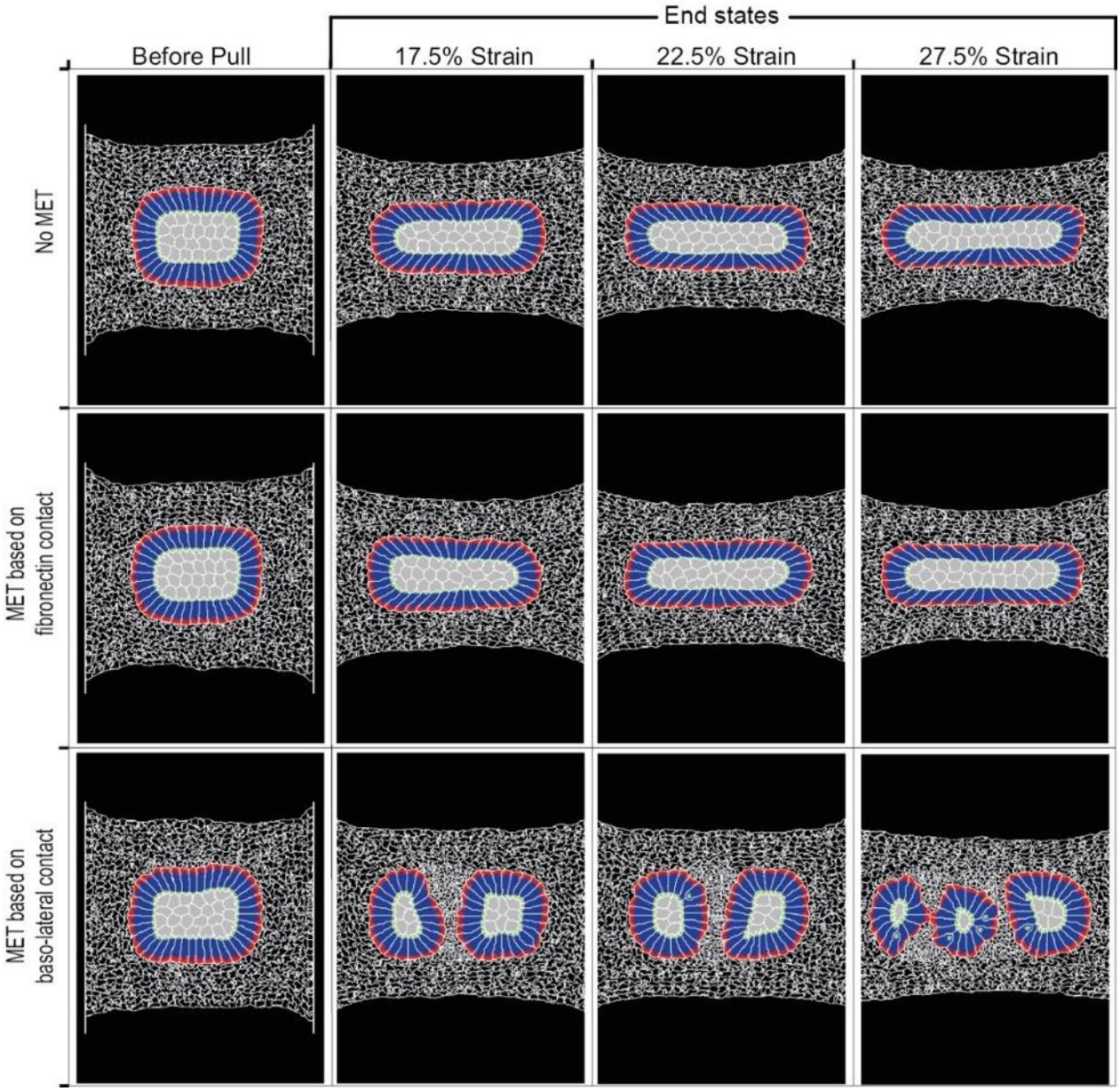

Fig S6: End states of simulations, testing different mesenchymal-epithelialization transition rules, related to Figure 5. Fully epithelialized somites were exposed to different strains (strain given by relative change in distance between movable walls), inducing aspect ratios of 2.5 (17.5% strain), 2.9 (22.5% strain) and 3.3 (27.5%) (compare Fig 3G). *Top row*: No MET was allowed after the pull. This was due to our initial hypothesis that somite doubling is nothing more than the reorganization of existing epithelial cells. We applied different strain values to see if high strain might lead to somite doubling. No somite division was observed. *Middle row*: MET was allowed after the pull if a cell had been in contact to the surrounding ECM matrix for a certain period of time. This MET rule did not allow somite division under various strain conditions. *Bottom row*: A new rule allows MET of mesenchymal cells upon contact to the lateral or basal membranes of epithelial cells. Formation of stable daughter somites could be observed.

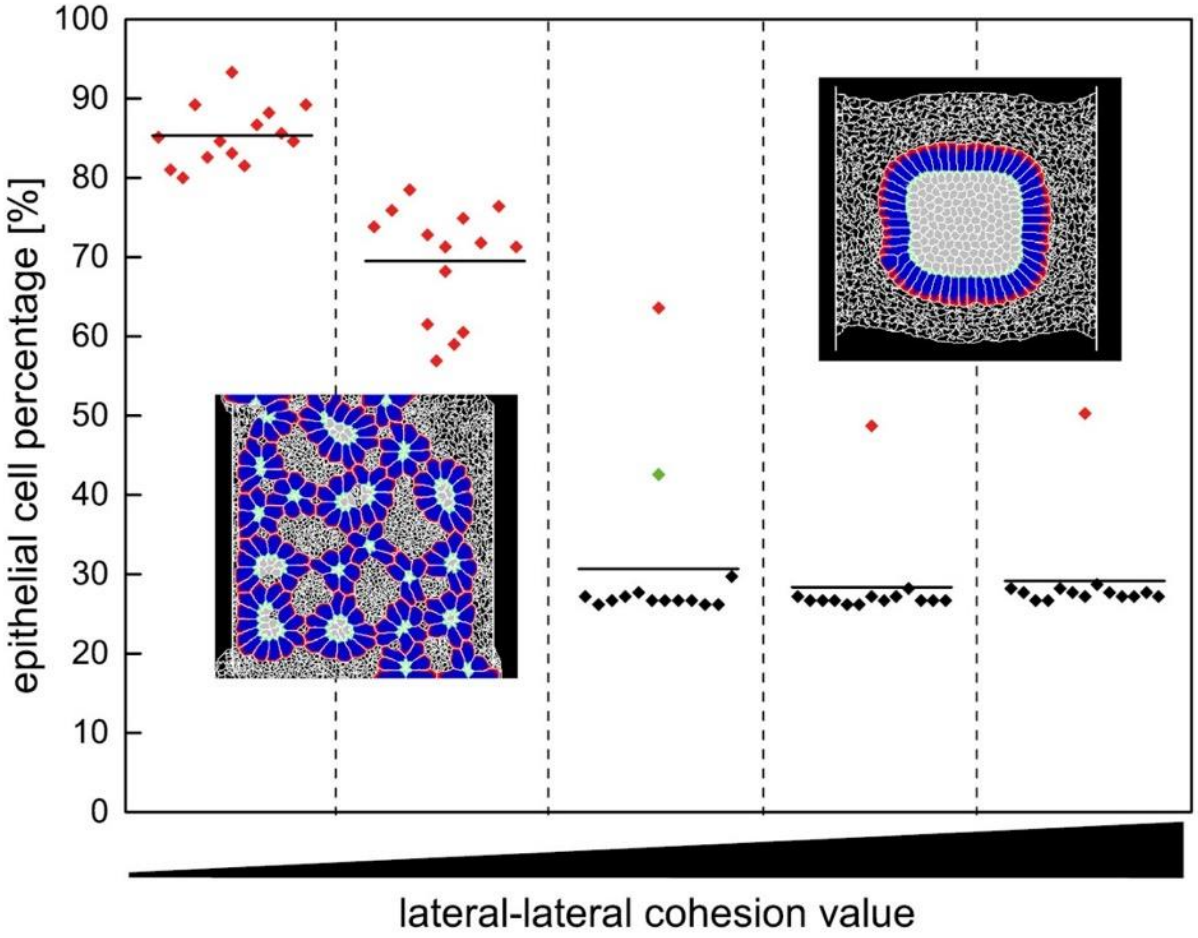

Fig S7: Influence of cohesion between lateral domains of epithelial cells on daughter somite number and epithelial cell percentages *in silico*, related to Figure 5. Cohesion between lateral domains of epithelial cells was varied in non-stretched somites to study the effect on somite formation. With low cohesion, almost 85% of mesenchymal cells became epithelial. This increase in epithelial cell number resulted in the formation of many epithelialized cell clusters (red data points), whereas for high cohesion values, we observed no somite division except for one case (green data point). Non-dividing somites are indicated by black data points.

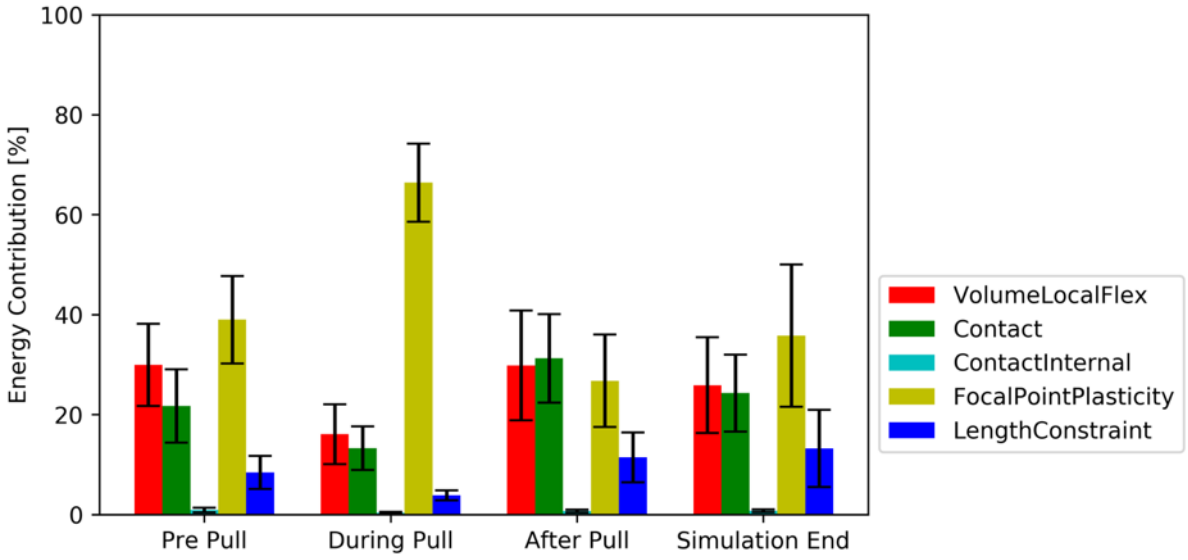

Fig S8: Contribution of the energy terms to the Hamiltonian, related to Figure 5. Terms are referred to by CompuCell3D plugin names; these are the software elements responsible the terms. The volume constraint (Eq. 3) restricts variations in the cell volume (VolumeLocalFlex). The contact energies (Eq. 2) are separated out for intercellular adhesion energy (Contact), i.e., contribution of cell-cell and cell-ECM adhesion and intracellular adhesion energy (ContactInternal), i.e., the adhesion between the compartments of the epithelial cells. The major contribution comes from the elasticity term (Eq. 4; FocalPointPlasticity). The elasticity term is responsible for the springs between the ECM volume elements and the springs between the compartments of the epithelial cells. The LengthConstraint plugin imposes elongation of a cell along an axis and ensures that cell elongation along the axis is closer to the target length. Shown are averages over n=14 simulations; error bars represent the 95% confidence interval.

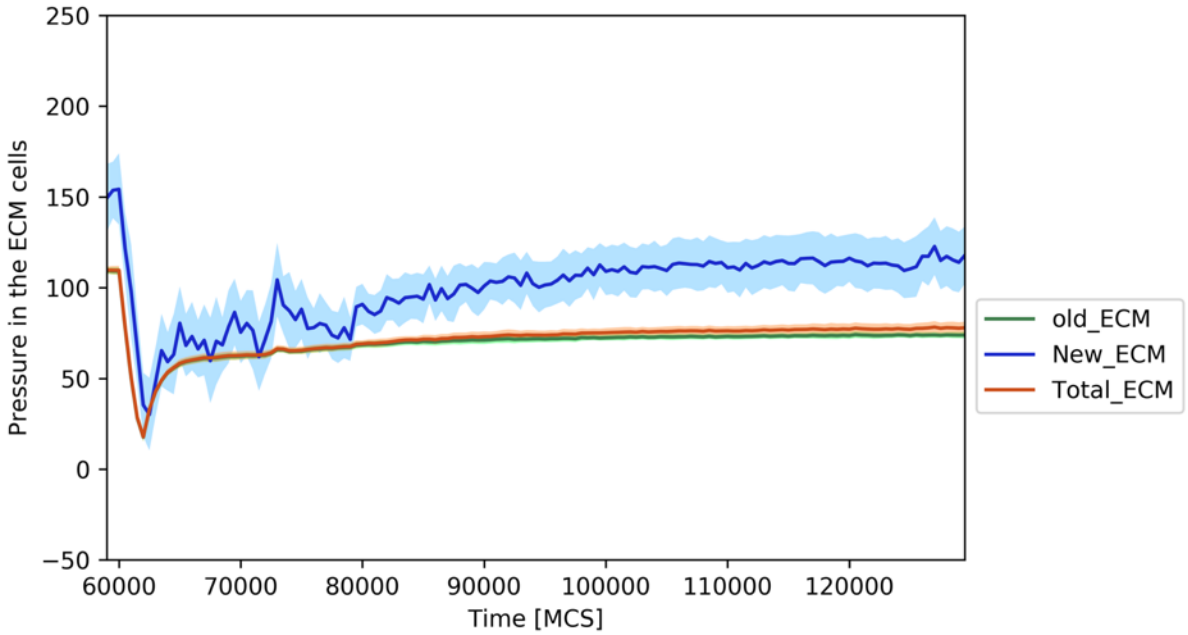

Fig S9: Pressure changes in the ECM cells over time, related to Figure 5. This plot shows pressure changes for old, new and total ECM during the simulation averaged over all cells in the simulation. At 60,000 MCS, axial outward pull is started. This pull brings the system under tension and causes a drop in the ECM pressure. After the pull, the ECM cells take some time to recover their pressure. However, only the newly formed ECM from the basal membranes of epithelial cells seems to have higher pressure. The newly formed ECM is the one which is secreted between the daughter somites whereas the old ECM is mainly on the outside. The dark lines show the average pressure over 14 simulations whereas slightly dull shaded area shows 95% confidence interval.

Supplemental tables

Table S1: Parameter values used in the Cellular Potts Model, related to Figure 5. Parameter values are given in simulation units and in the corresponding physical units, followed by a brief motivation. Energy (H) in the cellular Potts model relates to (cellular, adhesive, etc.) forces as $\vec{F} = \vec{\nabla} H$. Thus, estimates for the scaling of contact and elasticity energies to physical units can be based on measurements of the magnitude of the forces applied by the cells, the frequency by which pseudopods are extended and retracted ("Temperature"), the adhesion strengths between cells (see e.g., (Krieg et al., 2008)) and between cells and medium, combined with contact area, etc.

Parameter	**Value in simulation units**	**Physical units**	**Motivation**
Lattice spacing (Δx)	1 pixel width	0.5 μm	Chosen
Timestep	1 Monte Carlo Step (MCS)	0.36 s	Chosen
Lattice size	400 x 300 pixels	200 μm x 150 μm	Chosen
Cellular temperature	~100 energy unit (eu) per site update (i.e., 100 x lattice size eu / MCS = 12 x 10_6 eu/MCS)	-	Chosen; it reflects the rate of pseudopod extension and retraction and the forces that are applied
Somite diameter	~ 162 pixel widths	~ 80 μm	Somite is half the size of the *in vivo* somites (~160 μm) for simulation efficiency. The results are independent of simulation size
Total simulation steps	130,000 MCS	13:00 hours	Based on experiment
Start of pull	60,000 MCS	6:00 hours	Stabilisation of initial condition
Duration of pull	10,000 MCS	1:00 hours	Based on duration of single experimental pull
Epithelial target area V_{epi}	300 pixels (9% Apical, 70% Lateral and 21% Basal)	~ 75 μm_2	Measured using ImageJ from Kulesa and Fraser *Science* 2002 and Martins et al. PLOS ONE 2009[1]
Epithelial stiffness $\lambda_{volume-epi}$	100 energy unit (eu) per $pixel_2$	- (see Table caption regarding energy units)	Estimated based on experimental tissue organization
Mesenchymal target area V_{mes}	195 pixels	~50 μm_2	Measured using ImageJ from Martins et al. PLOS ONE 2009
Mesenchymal stiffness $\lambda_{volume-mes}$	30 eu/$pixel_2$		Estimated based on experimental tissue organization
ECM "cell" area	75 pixels	~20 μm_2	Chosen
ECM stiffness $\lambda_{volume-ecm}$	25 eu/$pixel_2$		Estimated based on experimental tissue organization
Epithelial polarization time	1500 MCS	~10 minutes	It takes 1 to 2 10-min t-frames in Video S3 of Martins et al. PLOS ONE 2009
Epithelial elongation time	1500 MCS	~10 minutes	*idem*
Epithelial sub-cellular spring stiffness	500 energy units per pixel width (eu/pw)	-	Estimated to approximate shape of epithelial cell

Apical-lateral spring length	15 pixel widths	7.5 µm	Estimated to approximate shape of epithelial cell
Apical – Basal spring length	30 pixel widths	15 µm	*As above*
Apical – Apical spring stiffness	100 energy units per pixel width (eu/pw)		*As above*
Apical – apical spring length	4 pixel widths	2 µm	*As above*
ECM-ECM spring stiffness	200 eu/pw	-	*As above*
ECM-ECM spring length	10 pixel widths	5 µm	*As above*
Contact energies			
Intercellular adhesion energies			
$J_{med-apical}$, $J_{med-lateral}$, $J_{med-basal}$, and $J_{med-mes}$	300 energy units per pixel width (eu/pw)	-	Estimated based on observed tissue organization, followed by sensitivity analysis (Fig. S7)
$J_{med-ecm}$	30 eu/pw	-	*As above*
$J_{apical-apical}$	3 eu/pw	-	*As above*
$J_{apical-lateral}$ and $J_{apical-basal}$	150 eu/pw	-	*As above*
$J_{apical-mes}$	160 eu/pw	-	*As above*
$J_{lateral-lateral}$	70 eu/pw	-	*As above*
$J_{lateral-basal}$	100 eu/pw	-	*As above*
$J_{lateral-mes}$	200 eu/pw	-	*As above*
$J_{lateral-ecm}$	130 eu/pw	-	*As above*
$J_{basal-basal}$	30 eu/pw	-	*As above*
$J_{basal-mes}$	280 eu/pw	-	*As above*
$J_{basal-ecm}$	40 eu/pw	-	*As above*
Internal adhesion energies between epithelial domains			
$J_{apical-lateral}$ and $J_{lateral-basal}$	2 eu/pw	-	*As above*
$J_{lateral-basal}$	20 eu/pw	-	*As above*

Transparent methods

Experimental Design

The objective of the study was to assess a possible role for mechanical strain in defining formation rate and total number of somites in a chick embryo. To that end we built an *ex ovo* embryo stretching device on top of our submerged filter paper sandwiches model and subjected young chick embryos to surplus axial tension (Fig 1). Deformations and possible changes to chick embryo morphology were recorded on-line by time-lapse imaging. To address specific questions, detailed imaging, immunohistochemistry and *in situ* hybridizations were performed after fixing of the embryos.

Embryo preparation and culture medium

Fertilized chicken eggs, white-leghorn, *Gallus gallus domesticus* (Linnaeus, 1758), were obtained from Drost B.V. (Loosdrecht, The Netherlands), incubated at 37,5°C in a moist atmosphere and automatically turned every hour. After incubation for approx. 33 h, HH8-9 chicken embryos were explanted using filter paper carriers (Chapman et al., 2001) and cultured *ex ovo* as modified submerged filter paper sandwiches (Fig 1A) (Chapman et al., 2001; Schmitz et al., 2016). Embryo culture medium consisted of Pannett-Compton (PC) saline (Pannett and Compton, 1924; Schmitz et al., 2016) mixed with freshly harvested thin albumen in a 3:2 ratio. PC stock solutions can be stored at 4 ºC for several months, but PC saline (mixture of stock solutions and MilliQ-water) should be prepared freshly every week and stored at 4ºC between experiments. Addition of Penicillin/Streptomycin (10000 U/ml) in 100x dilution prevents occasionally appearing bacterial infections. Silicone sheets further protected embryos in culture from infections as well as from convection of the medium. For the production of the silicon sheets, see Transparent Methods. Filter paper carriers were cut from thick filtration paper with a laser cutter according to the dimensions depicted in Figure 1D (Schmitz et al., 2016). Four holes were cut out from corners of the carriers (Fig 1D) to hook the filter paper sandwiches onto the pins of the motorized arms of the stretching setup (Fig 1A7, 1C).

Experimental setup - Embryo stretcher

Embryos were cultured and mechanically manipulated on a custom-made embryo stretcher (Fig 1). This setup allows to culture up to three embryos simultaneously in a variant of the earlier described “submerged filter paper sandwich” (Schmitz et al., 2016). The setup consists of a temperature-controlled medium container surrounded by a metal frame, which carries two motorized translation stages mounted on opposing sides. The stages were controlled by a custom-made LabVIEW routine, which allowed defining tension profiles for overnight experiments (see ‘Stretching protocol’ below). Embryos were fully submerged in the culture medium described above and the setup was prepared for an experiment as follows: The temperature-controlled beaker was placed in the centre of the motorized x-y-stage of the upright zoom microscope. Then the temperature-controlled beaker was filled with 200 mL of clean culture medium. The temperature of the beaker was set to 40°C and the silicone sheets were placed into the setup. Air bubbles were removed with a plastic transfer pipette. Then a chick embryo was explanted into a filter paper sandwich (Schmitz et al., 2016) (Fig 1A) and immediately submerged into the culture medium. After clamping three filter paper sandwiches into the setup, each filter sample was cut perpendicularly to the embryonic axis, about 1 mm posteriorly of the widest point of the elliptical aperture (dashed red line in Fig 1A-9). Then the culture medium was covered with 50 mL of light mineral oil using a plastic transfer pipette (Fig 1A-10).

Stretching protocol, axial deformation and somite deformation

Embryos were exposed to a standardized stretching protocol in the embryo stretcher (Fig 1C). In our original protocol, chick embryos were elongated at continuous speeds ranging from slow (1.3 µm/min, roughly matching the embryo’s natural elongation speed) to fast (8 µm/min). It was at 8 µm/min and after approx. 16 hours of stretching that we first observed the division of somites. However, embryos frequently ruptured, thus inhibiting a robust and repeatable observation of the phenomenon. In order to better study the dividing somites, we decided to take a different approach: We increased the stretching speed to 1.2 µm/s and applied the desired deformation during two relatively short stretching intervals (51 to 55 min) separated by a resting interval of two hours to allow damaged tissue to heal. During each stretching interval the displacement of the computer-controlled metal arm (see red arrow in Fig 1) extended the filter paper sandwiches by 3.8 mm at a speed of 1.2 µm/s. Subsequently, we calculated the resulting mechanical strain of the embryos for the first and the second stretching interval as relative length change compared to the axial length of the embryos before stretching. The first stretch led to 23 ± 3 % strain (average and standard deviation over 57 embryos); the second pull caused 19 ± 3 % strain.

Average somite formation period

To assess the hypothesized influence of mechanical tension on somitogenesis, we determined the average somite formation period for stretched and control embryos using our dark field microscopic time-lapse movies. We counted the number of somites in stretched embryos at the end of the second pull and at the end of the experiment. If a somite had not completely separated from the PSM at the end of the second pull, the counting was started after formation of the following somite. From the total number of somites formed after the application of the second pull and the corresponding time interval we calculated the average somite formation period. The somite formation period for control embryos was determined accordingly from the beginning of the culturing in the submerged filter paper sandwich.

Immunohistochemistry

After the pulling experiments, the embryos and age-matched controls were fixed in 4% paraformaldehyde overnight in PBS at 4$_{o}$C. Permeabilization in PBST + 0.15% Triton-X-100 lasted for 1.5 hours. Blocking was performed for 2 hours in PBST + 2% BSA + 5% normal goat serum. The following antibody was used: fibronectin mouse-anti-chicken (B3/D6-s, Hybridoma bank). The antibody was diluted in PBST with 1% BSA. Embryos were incubated in primary antibody solution for 24h at 4$_{o}$C, followed by extensive washing in PBS and incubation with appropriate Alexa Fluor-conjugated secondary antibody (1:500, Molecular Probes). Embryos were stained for F-actin using Alexa Fluor 546 Phalloidin (1:200, Molecular Probes) and for nucleic DNA using DAPI (1 µg/ml). Cell proliferation and apoptosis staining was performed using following antibodies: rabbit polyclonal anti-cleaved caspase-3 (1:200, Cell Signaling) and rabbit polyclonal anti-phosphohistone-H3 (1:400, Cell Signaling) with the appropriate Alexa Fluor-conjugated secondary antibodies (1:500, Invitrogen) and DAPI for nucleic DNA (1 µg/ml).

Proliferation rate and apoptotic rate

Apoptotic (Cas3 staining, control n=4, pulled n=4 embryos) and proliferating (pHH3 staining, control n=6, pulled n=6 embryos) cells in somitic mesoderm lanes (the newest somites I to VI) were counted in high-resolution confocal micrographs acquired on a Leica SP8 confocal microscope. At least 500 cells were counted per embryo. Apoptotic rate and proliferation rate were calculated as follows: (apoptotic/proliferation) rate (%) = number of positive staining cells/number of total cells×100.

Epithelial cell percentages

The percentage of epithelial cells in the equatorial z-plane of 13 daughter somite pairs, originating from the same mother somite, and 22 control somites was determined (*in vivo)*. To that end, high-resolution confocal micrographs of embryos stained with DAPI for nucleic DNA were acquired on a Leica SP8 confocal microscope. Then somites were counted for (mesenchymal) core cells and epithelial cells to calculate epithelial cell percentages. *In silico,* cell percentages in 12 daughter somite pairs and 12 control somites were counted accordingly.

Aspect ratio determination and ROC curve

The geometry of *in vivo* somites in controls and stretched embryos was described by measuring their length in rostro-caudal (x) and their width in medio-lateral (y) direction using the “Measure”-tool in ImageJ. Subsequently, the corresponding aspect ratio AR (AR = x/y) was calculated. Somites forming in controls and in stretched embryos after the second pull were measured upon their separation from the anterior tip of the PSM. Somites that had been formed before were measured at the end of the second pull. The aspect ratio of *in silico* somites was determined before and after the application of the pull accordingly (for strain regimes *in silico* see Cellular Potts model below).

Somite and somitocoel volume measurements

Z-stacks of somites V or VI in control and pulled embryos were acquired on a Leica SP8 confocal microscope. Stacks were obtained with 1 µm steps in z, with enough ventro-dorsal distance for imaging the whole mesoderm. The volumes of the whole somite or the somitocoel were compared between three groups: control, pulled somites that had not divided, and pulled somites that had divided (Fig 5I and 5J). To compare the somite and somitocoel volumes, the volumes were measured in fixed embryos. Confocal images were processed and converted with ImageJ (https://imagej.nih.gov/ij/). Manual segmentation, 3D reconstruction and volume analysis were then performed with 3D Slicer (https://discourse.slicer.org/), via the Segment Editor for segmentation, and Segment Statistics to calculate the volume. For the volumes of the divided somites/somitocoels, the volumes of both daughter somites were summed together. For statistical analysis, unpaired t-tests with Welch’s correction for standard deviation were performed with Graphpad.

In situ hybridizations

In situ hybridizations were performed by standard procedures. Embryos were fixed in freshly prepared 4% PFA in PBS. The embryos were pre-treated with proteinase-K in PBST at 37°C with agitation for 3 minutes. During staining, embryos were incubated in NTMT containing 4.5 µl NBT (75mg/ml in 70% DMF) and 3.5 µl BCIP (50mg/ml in 100% DMF) per 1.5 ml. Pulled embryos and age-matched controls were stained in the same wells for the same time, as much as possible. After the staining had been stopped, the embryos were photographed in glycerol 80% in H_2O with a Leica DFC320 camera on a Leica MZ75 microscope. Due to the relaxation of the stretched embryos, after their release from the embryo stretcher, the embryos tend to roll up. In order to photograph these embryos, they were placed on agar and below Corning cover glasses X2000 #1 (Fisher Scientific), with spacers and weights to hold them flat. This contributed to partly varying photo conditions for the in situ hybridization panels Fig 4H-M.

Cellular Potts model of somite division

To develop new hypotheses for the mechanisms underlying the somite division observed *in vivo*, we constructed a two-dimensional mathematical model based on the Cellular Potts Model (Glazier and Graner, 1993; Graner and Glazier, 1992), representing a cross-section through a three-dimensional somitic tissue. The model simulations were based on a Cellular Potts Model (CPM), also known as Glazier-Graner-Hogeweg model (Graner and Glazier, 1992). The model was implemented using CompuCell3D, an open source modelling package based on the CPM (Dias et al., 2014). The mesenchymal cells were modelled as regular cellular Potts cells, whereas for the epithelial cells we used a compartmental CPM (Dias et al., 2014), which represents biological cells as a collection of sub-cellular domains. The extracellular matrix was modelled as a collection of small volume elements connected to one another and to the epithelial cells by Hookean springs. Our compartmentalized CPM projects biological cells on a regular, square lattice as domains of (usually) connected lattice sites. Each lattice site, $\vec{x}$, corresponds to a cross-sectional area of approximately 0.5 µm × 0.5 µm and is associated with a domain index $\sigma(\vec{x}) \in \mathbb{Z}^{0,+}$ that uniquely identifies a whole cell, a cellular compartment, or a volume element of extracellular material. Cell identification number $\sigma = 0$ represents a generic 'medium'. Each domain σ has a type label $\tau(\sigma) \in \mathbb{N}$ to represent the generic 'type' (subcellular domain, ECM, and so forth) and an additional label $\xi\left(\sigma(\vec{x})\right) \in \mathbb{N}$ that bundles compartments to a biological cell or connected extracellular material. Although each individual object (subcellular compartment, ECM medium etc.) has its own unique domain index σ, many objects may be associated with the same type label τ, and many objects of the same of different type τ may form one biological object (e.g., an epithelial cell) with label ξ.

The evolution of our CPM is governed by a force-balance represented by Hamiltonian H:

$$H = H_{contact} + H_{volume} + H_{spring} \ , \qquad (Eq. 1)$$

which governs the dynamics of cells (e.g. cell behaviours, properties and interactions). Ignoring cell inertia, from this Hamiltonian the forces are recovered as $\vec{F} \propto \vec{\nabla} H$. The Hamiltonian is minimized using a Metropolis algorithm that mimics microscopic membrane and material fluctuations, such that both the equilibrium and the transient towards the equilibrium can be physically and biologically interpreted. $H_{contact}$ represents cell adhesion where cell-cell and cell-medium interactions take place through contact energies. The length of the interface between two cells defines the contact energy and is given by:

$$H_{contact} = \sum_{(\vec{x},\vec{x}')} J_{\tau(\sigma(\vec{x})),\tau\left(\sigma(\vec{x}')\right)} \left(1 - \delta_{\sigma(\vec{x}),\sigma(\vec{x}')}\right) \qquad (Eq. 2)$$

Here, $J_{\tau(\sigma(\vec{x})),\tau\left(\sigma(\vec{x}')\right)}$ is the bond energy between two neighbouring cell types $\tau(\sigma(\vec{x}))$ and $\tau(\sigma(\vec{x}'))$, and $\delta_{\sigma(\vec{x}),\sigma(\vec{x}')}$ is the Kronecker delta term in which adhesion is restricted to the cell membranes by eliminating the contribution from the neighbouring lattice sites belonging to the same cell. If $\sigma(\vec{x}) = \sigma(\vec{x}')$, the delta function returns a value of 1 and 0 otherwise. The term H_{volume} in the Hamiltonian specified in Eq. 1 is given by:

$$H_{volume} = \sum_{\sigma} \lambda_{volume}\,(\sigma).[v(\sigma) - V(\sigma)]^2 \qquad (Eq. 3)$$

and constrains the cell area, $v(\sigma)$, close to a resting area $V(\sigma)$. The Lagrange multiplier λ_{volume} represents cell elasticity - higher values of λ_{volume} reduce fluctuations of a cell's area from its target area.

Compartments of cells and subunits of the extracellular matrix can be mechanically coupled by Hookean springs that connect their centres of mass. Each spring contributes an additional energy bias H_{spring} to the Hamiltonian in Eq. S2, as

$$H_{spring} = \sum \lambda_{ij} \left(l_{ij} - L_{ij}\right)^2 \qquad (Eq. 4)$$

where l_{ij} is the absolute distance between the center of mass of cells i and j, and L_{ij} is a resting spring length. $\lambda_{ij}$is an elasticity parameter. Springs rupture if they exceed a threshold length; new springs are formed if cells move within a threshold distance. In our simulations, we have many cell types (epithelial internal compartments, extracellular matrix (ECM), and epithelial cell (apical)) which are connected using springs of which the parameters vary per cell type as explained in the Transparent Methods.

The CPM is updated using a Metropolis algorithm, which mimics the extension and retraction of pseudopods of the biological cells, and fluctuations of the extracellular matrix materials. The algorithm iteratively takes a randomly chosen lattice site $\vec{x}$ and attempts to copy its cell index $\sigma(\vec{x})$ into a randomly chosen adjacent lattice site $\vec{x}'$. This is called a copy attempt. The probability of accepting or rejecting the attempted copy is based on the energy minimization criteria and follows the Boltzmann probability,

$$P\left(\sigma(\vec{x}) \rightarrow \vec{x}'\right) = \begin{cases} 1 & ,\Delta H\left(\sigma(\vec{x}) \rightarrow \vec{x}'\right) < 0 \\ e^{\frac{-\Delta H\left(\sigma(\vec{x}) \rightarrow \vec{x}'\right)}{T}} & ,\Delta H\left(\sigma(\vec{x}) \rightarrow \vec{x}'\right) \geq 0 \end{cases} \qquad (Eq. 5)$$

where $\Delta H(\sigma(\vec{x}) \rightarrow \vec{x}')$ represents the change in the Hamiltonian due to the copy attempt. If the attempted copy update would reduce the energy, i.e. $\Delta H(\sigma(\vec{x}) \rightarrow \vec{x}') < 0$, the update is accepted with a probability of 1. If the energy increases due to the copy-attempt, the system follows Boltzmann probability to accept or reject a copy-attempt. The parameter T is the cellular temperature, representing the amplitude of active cell membrane fluctuations or fluctuations of the extracellular materials. Simulation time proceeds in *Monte Carlo Steps* (MCS); One MCS corresponds to 0.36 seconds of experimental time, and consists of *N* copy attempts, with *N* the number sites in the lattice. All parameters are given in dimensionless units in Table S1 alongside interpretation in terms of physical units and a brief motivation for the values used. Further model assumptions, a detailed description of the somite stretching protocol, a study of the relative contributions of the mechanisms represented by the Hamiltonian, and a parameter sensitivity analysis are in the Supplemental Materials.

Statistical Analyses

For assessing epithelial cell percentage in the somites, statistical analysis was performed using GraphPad Prism software. Unpaired parametric two tailed t-tests (with Welch's correction for unequal variance) were applied to determine P-values for the epithelial percentages shown in the graph in Fig 3E. The percentages of epithelial cells change significantly *in vivo* (P<0.0001) and *in silico* (P<0.0001).

Statistical analyses of the proliferation and apoptosis rates were performed using GraphPad Prism software. Mann–Whitney unpaired non-parametric two-tail testing was applied to determine the P-values for the apoptotic and proliferation rates, respectively. shown in Fig 5F.

The receiver operating characteristics (ROC) curves (Hanley and McNeil, 1982) (Fig 3H) were generated by performing a binary logistic regression using the Data Analysis Tool of the Real Statistics Excel plugin Realstats (available at http://www.real-statistics.com). We analysed how well the aspect ratio of stretched somites *in vivo* and *in silico* can predict the binary outcome of whether a somite will undergo division or not. This is measured by the area under the curve (AUC) in the ROC diagram. The AUC can vary between 0.5 (stochastic relation) and 1 (fully determined). 95% Confidence intervals for AUC values were calculated using the 'ROC curve analysis' tool of MedCalc software (available at https://www.medcalc.org/index.php).

Silicone sheets

Silicone sheets protected embryos in culture from convection of the medium, thereby avoiding additional damage. Silicone sheets (ca. 350 µm in thickness) were made using a Sylgard® 184 Silicone Elastomer Kit as follows: A 15-cm plastic petri dish was placed on a scale and 6.165 g (5.554 mL) of base solution were pipetted into its centre using a plastic transfer pipette (cut off tip). Then 0.206 g (0.2 mL) of curing agent were added using a glass pipette. Base and curing agent were mixed slowly, using a wooden spatula and spread out over the bottom of the petri dish. The petri dish was placed into a vacuum chamber for 2 hrs to remove air bubbles and let silicone solution spread out equally. Exposure to 80 °C for ca. 2 hrs let silicone polymerize and cure. Afterwards, silicone was let to cool to room temperature for about 5 hrs or overnight. Tweezers were used to free the borders of the silicone sheet from the walls of the petri dish and peel the sheet from the culture dish (wear gloves). Silicone was stored between sheets of a plastic document sleeve to prevent accumulation of dust. For preparing silicone sheets fitting in the setup, the plastic sleeve was removed from one side of the silicone sheet and the plastic stencil (Fig 6D) placed on it. A razor blade was used to cut around the outline of the stencil and the ten holes indicated by the stencil were cut out using a

hole puncher. After removing the other plastic sleeve layer, silicone sheets were stored in a closed 10 cm petri dish.

Cellular Potts Model assumptions

The model included the following assumptions: (i) the tissue surrounding the somite can be approximated as elastic, and was modelled as a non-specified extracellular matrix (ECM); (ii) the somite consists of polarized epithelial cells forming the outer layer (Dias et al., 2014), and the somite core (somitocoel) consists of unpolarized mesenchymal cells. The mesenchymal cells in the core of the somite were represented by single-compartment, non-coupled and non-polarized cells. Following Dias *et al.* (Dias et al., 2014) the epithelial cells in our model consisted of three domains, called 'apical', and 'lateral' and 'basal' (Fig S5). The three compartments were initially distributed at random inside an epithelial cell and after a brief relaxation period of 1500 MCS (epithelial polarization time), these compartments were connected internally to one another using linear elastic springs (Eq. 4). To achieve epithelial elongation, target lengths of all internal springs ($L_{apical-lateral}$, $L_{apical-basal}$, $L_{lateral-basal}$) were individually incremented by 1 every 20th MCS within the elongation time frame (1500 MCS, approximately 9 min), until every spring reached its final specified target length ($L_{apical-lateral} = 15, L_{apical-basal} = 30,\ L_{lateral-basal} = 20$). We have used springs between adjacent cells (such as apical compartments of epithelial cells or ECM cells) to represent strong Cadherin or tight junctions. Within one epithelial cell, springs are used to make epithelial cells elongated and to have domains with different adhesion properties. These assumptions have been adapted from (Dias et al., 2014). The ECM, with its main functional component fibronectin *in vivo* (Rifes and Thorsteinsdóttir, 2012), was modelled as a network of compartments connected by Hookean springs of resting length $L_{ecm-ecm} = 10$ with elastic stiffness $\lambda_{ecm-ecm} = 200$. These parameters were chosen such that the ECM stays intact during and after stretching.

We first attempted to construct a well-organized, initial epithelial structure as a starting point for the stretching model. Contact energies between domains as well as contact energies with other cell types and the ECM were set according to Table S1. In absence of quantitative values for the adhesion strengths and interfacial tensions between the cells, we estimated parameter values for which a stable epithelial monolayer is maintained in our simulations, followed by parameter sensitivity studies. We assumed the apical domains of adjacent epithelial cells cohered strongly, following Dias *et al.*'s assumption mimicking the distribution of N-Cadherin *in vivo* (Dias et al., 2014). The lateral domains of epithelial cells (between the apical and basal domains) adhere strongly to each other, similar to Cadherin mediated cohesion *in vivo* (Horikawa et al., 1999). To represent the apical actin ring, each centre of mass of an apical unit was connected to the centre of mass of neighbouring apical domains on either side (left and right) using elastic springs of a resting length of $L_{ij} = 4$ with elastic stiffness $\lambda_{apical-apical} = 100$.

The monolayer of epithelial cells was constructed by initializing the simulation with a collection of mesenchymal cells surrounded by an elastic ECM. We selected a mesenchymal cell at the boundary with the surrounding ECM and made it epithelial. This first epithelialized cell induced MET in neighbouring cells based on basolateral contact (Jackson et al., 2017) where MET was implemented by turning over a mesenchymal cell into a compartmentalized, unpolarized epithelial cell. Subsequent MET of the adjacent mesenchymal cells finally led to a fully epithelialized somite-like structure. After a stable, somite-like, epithelial structure had formed, we gradually strained the extracellular matrix in our simulations, in order to mimic the experimental setup. To this end, we connected two 'walls' constructed out of immobile cells to the left and right-hand ends of the ECM using stiff elastic springs and slowly moved the walls apart by 1 pixel every 50 MCS (~ 1.7µm/min), similar to the compression of tissue spheroids (Marmottant et al., 2009)and the application of stents in arteries (Tahir et al., 2015).

Somite stretching in silico

The stretching rate was sufficiently slow (walls moved outward by 1 pixel every 50 MCS, corresponding to ~ 1.7µm/min), such that it did not damage the ECM cells (Movie S3). Upon stretching, several springs between neighboring apical compartments released and mesenchymal cells from the core became exposed to the lateral or basal membranes of epithelial cells leading to additional MET. These additional epithelial cells disturbed the equilibrium and could not get incorporated into the original epithelial ring. So, the epithelium started to reorganize and divide into daughter somites (Fig S6, bottom row and Movie S3). To systematically analyse how well the geometry of stretched somite predicts division we increased the distance between the lateral walls slowly by 30 to 110 pixels (corresponding to 15 µm to 55 µm), resulting into aspect ratio values similar to stretched somites *in vivo* (Fig 5G).

Fibronectin deposition

Based on our observations that daughter somites are separated and presumably stabilized by a newly forming fibronectin matrix (Fig 3), we implemented a similar rule for ECM production by the basal units of epithelial cells. If the basal domain of an epithelial cell is not attached to a specified amount of ECM (given by threshold value) for a certain duration, it produces an additional ECM cell. This production continues until the threshold value is reached again. Such production of the fibronectin allows the dividing somites to separate from each other permanently.

Parameters
The parameters used in the simulations are listed in Table S1, alongside their interpretation in terms of physical units and a brief motivation.

Model validation
The *in silico* somite model can be parameterized to the experimentally observed ratio of mesenchymal and epithelial cells**.** Following the MET based on the basolateral contact rule, we observed that initial epithelialization of the somite and division of the somites after stretching can be achieved both with a large core and small core somite. To further validate the *in silico* model, we also tested the influence of decreased cohesion between lateral domains of epithelial cells in epithelializing, non-stretched somites. Similar to results in *N-Cadherin/cad11* double-homozygous mouse mutants (Horikawa et al., 1999), we observed subdivisions into small cell clusters of epithelioid morphology (Fig S7).

Energy
We also tested the relative contribution of each energy term in time at different stages in the simulation (Fig. S8). The elasticity terms (Eq. 4) have a major contribution towards the overall system energy. This is responsible for all the inter- and intracellular springs in the model. The contribution of elasticity is substantially higher during the pull and also higher during pre-pull and at the end of simulations.

Pressure changes
From Fig S7, one can see small ECM cells between the daughter somites. This suggests a slightly higher pressure in middle of the daughter somites, which could be due to the production of the new ECM cells from the basal membranes of epithelial cells. In order to evaluate the pressure changes in the ECM cells, we estimated the pressure in the ECM cells over time using:

$$\mathcal{P} = 2\lambda(\mathrm{V_i} - \mathrm{v_\sigma})$$

where $\mathrm{V_i}$ is the target volume and $\mathrm{v_\sigma}$ is the current cell volume. λ is an inelasticity constant. Fig S9 shows that axial pull initially causes a drop in the ECM cell pressure, but after some time the pressure was regained. The newly formed ECM cells initially have a higher pressure than the old ECM cells. This is because the whole system is continuously under tension and ECM acts like a spring mesh. Since there is no empty space for new cells inside the ECM mesh, it takes time for new ECM cells to achieve or maintain their volume. For this reason, new ECM cells are under slightly more pressure than the old ECM cells.

Supplemental References

Chapman, S.C., Collignon, J., Schoenwolf, G.C., Lumsden, A., 2001. Improved method for chick whole-embryo culture using a filter paper carrier. Dev. Dyn. 220, 284–289. https://doi.org/10.1002/1097-0177(20010301)220:3<284::AID-DVDY1102>3.0.CO;2-5

Dias, A.S., de Almeida, I., Belmonte, J.M., Glazier, J.A., Stern, C.D., 2014. Somites Without a Clock. Science (80-.). 343, 791–795. https://doi.org/10.1126/science.1247575

Glazier, Graner, 1993. Simulation of the differential adhesion driven rearrangement of biological cells. Phys. Rev. E. Stat. Phys. Plasmas. Fluids. Relat. Interdiscip. Topics 47, 2128–2154.

Graner, F., Glazier, J.A., 1992. Simulation of Biological Cell Sorting Using a 2-Dimensional Extended Potts-Model. Phys. Rev. Lett. 69, 2013–2016. https://doi.org/10.1103/PhysRevLett.69.2013

Hanley, A.J., McNeil, J.B., 1982. The Meaning and Use of the Area under a Receiver Operating Characteristic (ROC) Curve. Radiology 143, 29–36. https://doi.org/10.1148/radiology.143.1.7063747

Horikawa, K., Radice, G., Takeichi, M., Chisaka, O., 1999. Adhesive Subdivisions Intrinsic to the Epithelial Somites. Situ 215, 182–189. https://doi.org/10.1006/dbio.1999.9463

Jackson, T.R., Kim, H.Y., Balakrishnan, U.L., Stuckenholz, C., Davidson, L.A., 2017. Spatiotemporally Controlled Mechanical Cues Drive Progenitor Mesenchymal-to-Epithelial Transition Enabling Proper Heart Formation and Function. Curr. Biol. 27, 1326–1335. https://doi.org/10.1016/j.cub.2017.03.065

Krieg, M., Arboleda-Estudillo, Y., Puech, P.H., Käfer, J., Graner, F., Müller, D.J., Heisenberg, C.P., 2008. Tensile forces govern germ-layer organization in zebrafish. Nat. Cell Biol. 10, 429–436. https://doi.org/10.1038/ncb1705

Marmottant, P., Mgharbel, A., Kafer, J., Audren, B., Rieu, J.-P., Vial, J.-C., van der Sanden, B., Maree, A.F.M., Graner, F., Delanoe-Ayari, H., 2009. The role of fluctuations and stress on the effective viscosity of cell aggregates. Proc. Natl. Acad. Sci. U. S. A. 106, 17271–17275. https://doi.org/10.1073/pnas.0902085106

Pannett, C., Compton, A., 1924. the Cultivation of Tissues in Saline Embryonic Juice. Lancet 203, 381–384. https://doi.org/10.1016/S0140-6736(01)15954-4

Rifes, P., Thorsteinsdóttir, S., 2012. Extracellular matrix assembly and 3D organization during paraxial mesoderm development in the chick embryo. Dev. Biol. 368, 370–81. https://doi.org/10.1016/j.ydbio.2012.06.003

Schmitz, M., Nelemans, B., Smit, T.H., 2016. A submerged filter paper sandwich for long-term ex ovo time-lapse imaging of early chick embryos. J. Vis. Exp. 54636. https://doi.org/10.3791/54636

Tahir, H., Niculescu, I., Bona-Casas, C., Merks, R.M.H., Hoekstra, A.G., 2015. An in silico study on the role of smooth muscle cell migration in neointimal formation after coronary stenting. J. R. Soc. Interface 12, 20150358.